

Comparative Whole Metagenome Analysis in *JID Open* Lesional and Nonlesional Scalp Areas of Patients with Psoriasis Capitis and Healthy Individuals

Britta De Pessemier¹, Celia Díez López¹, Steff Taelman^{2,3}, Merel Verdonck¹, Yang Chen^{4,5,6}, Annelies Stockman⁷, Jo Lambert⁸, Tom Van de Wiele¹ and Chris Callewaert¹

Psoriasis is an immune-mediated inflammatory disorder, where the majority of the patients suffer from psoriasis capitis or scalp psoriasis. Current therapeutics remain ineffective to treat scalp lesions. In this study, we present a whole-metagenome characterization of the scalp microbiome in psoriasis capitis. We investigated how changes in the homeostatic cutaneous microbiome correlate with the condition and identified metagenomic biomarkers (taxonomic, functional, virulence factors, antimicrobial resistance genes) that could partly explain its emergence. Within this study, 83 top and back scalp samples from healthy individuals and 64 lesional and nonlesional scalp samples from subjects with untreated psoriasis capitis were analyzed. Using qPCR targeting the 16S and 18S ribosomal RNA genes, we found a significant decrease in microbial load within scalp regions affected by psoriasis compared with that in their nonlesional counterparts. Metagenomic analysis revealed that psoriatic lesions displayed significant lower *Cutibacterium* species (including *C. modestum*, *C. namnetense*, *C. granulosum*, *C. porci*), along with an elevation in *Staphylococcus aureus*. A heightened relative presence of efflux pump protein-encoding genes was detected, suggesting potential antimicrobial resistance mechanisms. These mechanisms are known to specifically target human antimicrobial peptides (including cathelicidin LL-37), which are frequently encountered within psoriasis lesions. These shifts in microbial community dynamics may contribute to psoriasis disease pathogenesis.

Keywords: Metagenomics, Pathogenomics, Psoriasis capitis, Scalp microbiome, Skin microbiome

Journal of Investigative Dermatology (2024) ■, ■–■; doi:10.1016/j.jid.2024.07.020

INTRODUCTION

Scalp psoriasis or psoriasis capitis occurs in 80% of the patients with psoriasis (Ortonne et al, 2009), and nonscarring alopecia areata (hair loss) often coincides with it (George et al, 2015; van de Kerkhof and Franssen, 2001). Psoriasis affects 2–3% of the global population (Lebwohl, 2003), with a higher prevalence in western countries (eg, 3.1% in Italy, 8.5% in Norway, and 2–3% in the United States) than non-western countries (eg, 0–0.49% in African, Asian, indigenous Latin Americans, and Native Americans) (Armstrong

et al, 2021; Parisi et al, 2013). Psoriasis vulgaris, the most prevalent form, is characterized by epidermal hyperproliferation and immature differentiation of keratinocytes in the basal layer of the skin, resulting in demarcated regions of skin redness and hardened plaques covered with silvery scales (Greb et al, 2016). Seborrheic dermatitis and psoriasis share clinical similarities because these are both inflammatory skin disorders that may affect the scalp area among other body sites (Dessinioti and Katsambas, 2013). Seborrheic dermatitis is typically distinguished by yellow and greasy scales (Kim et al, 2013). Psoriatic lesions may sometimes co-occur with seborrheic dermatitis lesions; this pathology has been described as seboporiasis or seborrhiasis (van de Kerkhof and Franssen, 2001).

The complex and multifactorial nature of psoriasis contributes to existing gaps in our understanding of its pathogenesis. Topical treatments of psoriasis include topical corticosteroids, vitamin D analogs, keratolytic agents, imidazole antifungals, and calcineurin inhibitors (Armstrong and Read, 2020; van de Kerkhof and Franssen, 2001). However, therapeutic treatments often remain ineffective to cure the scalp lesions (Hjuler et al, 2019; Papp et al, 2007). Emerging evidence highlights the important role of the scalp microbiome in the aggravation of psoriasis capitis, which presents a potential therapeutic avenue (Ainali et al, 2012; Boehncke and Schön, 2015). The human skin is covered with billions

¹Center for Microbial Ecology and Technology, Ghent University, Ghent, Belgium; ²Department of Data Analysis and Mathematical Modelling, Ghent University, Ghent, Belgium; ³BIOLIZARD, Ghent, Belgium;

⁴Department of Dermatology, School of Medicine, University of California San Diego, California, USA; ⁵Department of Pediatrics, School of Medicine, University of California San Diego, California, USA; ⁶Biomedical Sciences Graduate Program, University of California San Diego, California, USA;

⁷Department of Dermatology, AZ Delta, Torhout, Belgium; and

⁸Department of Head & Skin, Ghent University, Ghent, Belgium

Correspondence: Chris Callewaert, Center for Microbial Ecology and Technology, Ghent University, Campus Coupure, Coupure Links 653, Gent 9000, Belgium. E-mail: Chris.Callewaert@UGent.be

Abbreviations: AMP, antimicrobial peptide; AMR, antimicrobial resistance; FDR, false discovery rate; RND, resistance nodulation division; rRNA, ribosomal RNA; VF, virulence factor

Received 12 April 2024; revised 20 June 2024; accepted 8 July 2024; accepted manuscript published online XXX; corrected published online XXX

of microbes, comprising a diverse community of bacterial, fungal, microeukaryotic (mites), archaeal, and viral species, including phages that reside on the skin surface and in its deeper layers (Skowron et al, 2021). These microorganisms collectively form a complex ecosystem often referred to as the second skin (Eisenstein, 2020). The commensal microorganisms inhabiting the harsh, acidic, and nutrient-poor environment of our skin play a crucial role in protecting us from harmful pathogenic species, maintaining a functional skin barrier, and modulating the host's innate and adaptive immune response (Chen et al, 2018). Furthermore, the skin microbial community exhibits site-specific biogeographical characteristics (Human Microbiome Project Consortium, 2012; Costello et al, 2009; Grice et al, 2009; Oh et al, 2014). The scalp is a distinct area on the body rich in sebaceous glands, which produce sebum to moisturise and protect the region, serving as an antibacterial barrier (Grice and Segre, 2011).

Several studies have revealed alterations in the composition and diversity of the skin microbiome in individuals with psoriasis (Choi et al, 2022; Gao et al, 2008; Raza et al, 2007; Rudramurthy et al, 2014; Tett et al, 2017; Tomi et al, 2005). Culture-dependent studies have demonstrated that *Staphylococcus aureus*, *Streptococcus pyogenes*, and *Malassezia* spp. are linked to psoriasis flare up (Raza et al, 2007; Rudramurthy et al, 2014; Tomi et al, 2005). However, these studies have the limitation that numerous species are viable but nonculturable and remain undetectable using traditional culturing techniques. Culture-independent techniques, such as amplicon sequencing of ribosomal marker genes (eg, 16S, internal transcribed spacer, and 18S ribosomal RNA [rRNA]), have broadened our understanding of the microbial communities inhabiting us, collectively called the human microbiome (Turnbaugh et al, 2007). Choi et al (2022) studied the scalp microbiome of patients with psoriasis by targeting the V3 region of the 16S rRNA gene and demonstrated an increase of *Pseudomonas* with psoriasis severity (Choi et al, 2022). Imidazole treatment in patients with psoriasis capitis successfully resolved psoriatic scalp lesions, suggesting a role of the fungal microbiome (van de Kerkhof and Franssen, 2001). Inconsistent variations in the fungal microbial community, targeting the 18S rRNA and internal transcribed spacer region, were reported between individuals with psoriasis and healthy controls (Paulino et al, 2006). The study of Takemoto et al (2015) reported a higher diversity in the fungal microbiome of patients with psoriasis than in healthy controls and a lower overall abundance of *Malassezia*. Other studies reported *M. restricta* to be the dominant species in patients with psoriasis (Paulino et al, 2006; Takemoto et al, 2015). Despite the advantages, the taxonomic resolution remains constrained owing to the limited sample sizes or nonoptimal sequencing quality that practically limits phylogenetic characterization to the genus level (Johnson et al, 2019). In addition, the biological function of taxa identified within a community can only be predicted, using tools such as Picrust or Tax4Fun (Aßhauer et al, 2015; Langille et al, 2013), because the rRNA gene is a taxonomic marker.

Shotgun metagenomic sequencing or whole-metagenome sequencing allows the study of the taxonomic composition

and functional potential of complex microbial communities covering human, natural, and animal environments, including the skin (Human Microbiome Project Consortium, 2012; Grice et al, 2009; Grice and Segre, 2011; Oh et al, 2014). The study by Tett et al (2017) revealed the skin microbiome's strain-level composition associated with psoriasis at the retroauricular crease (scalp adjacent skin area) and elbow sites. They demonstrated a reduction in microbial diversity at the retroauricular crease lesional sites, alongside an elevation in *Staphylococcus* abundance (Tett et al, 2017). Expanding on the valuable insights gained from these pivotal studies, our study employed a comprehensive approach to investigate the taxonomic and functional characteristics of the scalp microbiome in both healthy individuals and those afflicted with psoriasis capitis. We assessed both metagenomic-assembled genomes and microbial isolate genomes for improved taxonomic profiling. Our research significantly contributes to the understanding of scalp microbial profiles and functionalities in the context of psoriasis capitis, providing valuable insights into the interplay between the microbiome and this dermatological condition and providing, to our knowledge, previously unreported avenues for potential therapeutic approaches.

RESULTS

Differential microbiota abundance in psoriasis lesions versus healthy scalps

The microbiome of 33 untreated patients was investigated, all of whom were clinically diagnosed with psoriasis capitis. Samples were collected from lesional and nonlesional scalp areas. In addition, 43 healthy participants were sampled, where samples of the top and back of the scalp were taken (Figure 1 and Supplementary Tables S1 and S2).

We observed that the number of nonhuman-sequenced reads was significantly (false discovery rate [FDR] < 0.0001) lower in diseased lesional scalp areas than in their nonlesional counterparts and healthy top and back scalp areas (Figure 2a and Supplementary Figure S1). Through the application of qPCR targeting the 16S rRNA gene and 18S rRNA gene, normalized by the number of human housekeeping *ACTB* gene copies, we observed a significant (FDR < 0.0001) decrease in the number of 16S rRNA/*ACTB* and 18S rRNA/*ACTB* gene copies in lesional scalp areas compared with those in nonlesional scalp areas (Figure 2b and c). A significant (FDR < 0.0001) reduction in the estimated number of reads coming from bacteria and eukaryotes was observed in lesional scalp areas compared with that in nonlesional, top, and back scalp areas (Supplementary Figures S2 and S3). No significant differences in microbial reads were observed among the top, back, and nonlesional scalp areas (Figure 2a).

Higher Bray–Curtis dissimilarity and reduced species richness observed in psoriasis lesions relative to those in healthy scalp

Bray–Curtis distances were calculated to compare metagenomes among distinct participants from the same site (interindividual dissimilarities), within each participant (intraindividual dissimilarities), and between different sites (body-site dissimilarities) (Figure 3 and Supplementary Figure S4a). Healthy top and back scalp areas demonstrated significantly (FDR < 0.0001) lower dissimilarity than

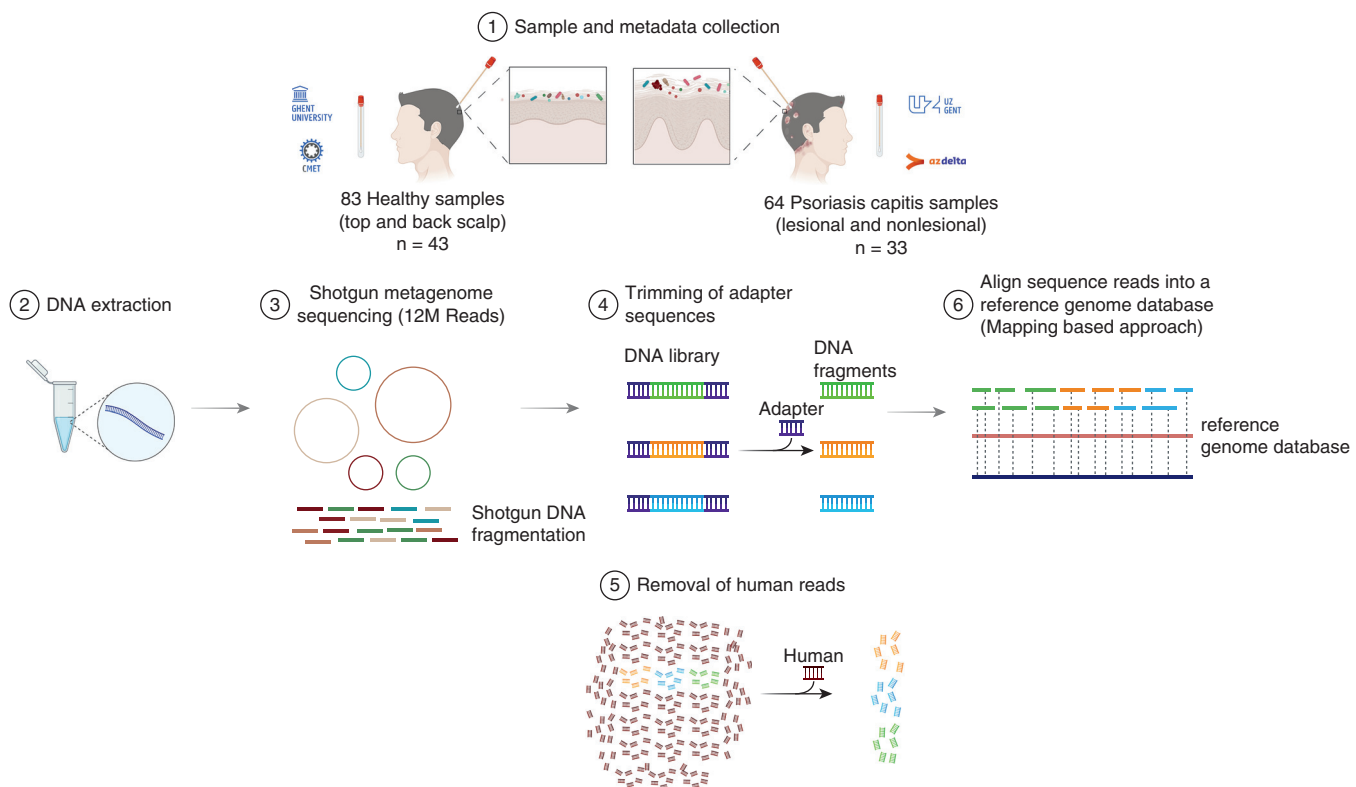


Figure 1. Chronological overview of the study. A total of 83 healthy (top and back scalp, n = 43) and 64 psoriasis capitis (lesional and nonlesional, n = 33) samples were collected, including associated metadata of the participants. (1) Psoriatic epidermis demonstrates pronounced epidermal acanthosis, hyperkeratosis, and elongation of rete ridges; (2) DNA was extracted; (3) shotgun metagenome sequencing or WMS (12 million reads); (4) trimming of adapter sequences and (5) removal of human reads; and (6) reads were aligned against the reference genome database. WMS, whole metagenome sequencing. Created in Biorender. De Pessemier, B. (2023) BioRender.com/f63l201.

psoriasis lesional and nonlesional scalp areas (Figure 3a). Lesional areas displayed significantly (FDR < 0.001) higher dissimilarity than nonlesional areas in patients with psoriasis

(Figure 3a). This suggests that healthy scalp regions exhibit more consistent microbial compositions across individuals than psoriasis-affected areas.

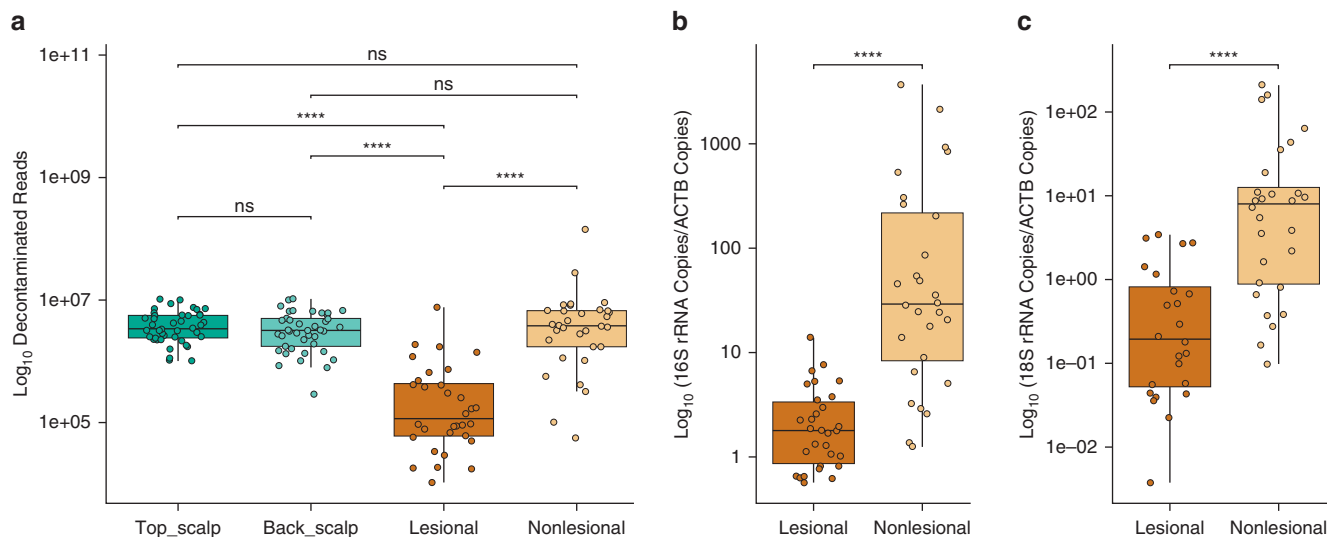


Figure 2. Comparison of microbial load in different scalp skin sites. Boxplots (line indicates median; boxes represent first and third quartiles) show, for each scalp skin site, on a log₁₀ transformed y-axis, (a) the number of decontaminated reads after mapping the trimmed reads against the human reference genome database (hg37) with Bowtie2, (b) the number of 16S rRNA/ACTB copies, and (c) the number of 18S rRNA/ACTB copies. Sites are colored by site characteristic: top and back scalp areas from healthy participants and lesional and nonlesional scalp areas from participants with psoriasis capitis. A nonparametric Wilcoxon test was performed. Asterisks indicate the significance level of the FDR-adjusted P-values: ****P < .0001, ***P < .001, **P < .01, and *P < .05. FDR, false discovery rate; ns, nonsignificant; rRNA, ribosomal RNA.

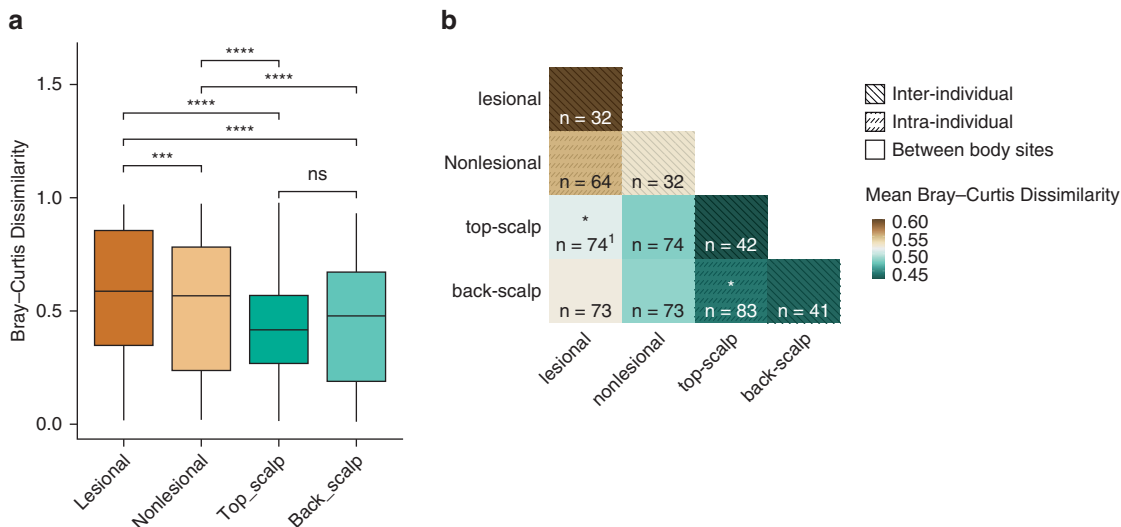


Figure 3. Bray–Curtis dissimilarity among scalp skin sites. (a) Boxplots (line indicates median; boxes represent first and third quartiles) of interindividual Bray–Curtis dissimilarities between samples based on relative abundance of metagenomic species, stratified by sample origin: lesional, nonlesional, healthy top scalp, and healthy back scalp areas. Pairwise comparisons were calculated using the Wilcoxon signed rank test. (b) Beta–diversity matrix based on mean values of Bray–Curtis distances of metagenomics samples from the same patient (intra–beta-diversity), between patients (inter–beta-diversity), and between body sites. N indicates the number of samples included. The values along the diagonal correspond to the mean Bray–Curtis dissimilarity between samples collected from different individuals originating from a comparable anatomical region. This provides insight into the degree of dissimilarity between individuals with respect to their microbial composition at the specific body site under investigation (interindividual variability). Lower values along this diagonal indicate higher similarity in microbial compositions among samples from distinct individuals within the group.¹ Adonis2 was performed; however, the assumption of homoscedasticity (homogeneous dispersion) was not met. Hence, the significant results that were obtained with adonis2 could be an artifact of the heterogeneous dispersions.

For healthy individuals, top and back scalp samples exhibited lower Bray–Curtis dissimilarity than lesional and nonlesional samples from patients with psoriasis (intra-individual variability) (Figure 3b), indicating a shift in microbial composition influenced by health status. Although the body-site factor demonstrated a significant ($FDR < 0.05$) effect between top and back scalp areas, the model had low prediction accuracy ($R^2 = 0.02394$), indicating that the majority of the variance remained unexplained (Supplementary Tables S3 and S4). This suggests that top and back scalp contained a reasonably similar microbial community. Intra-individual variability analysis revealed that individual-specific attributes significantly ($FDR < 0.01$) contributed to variations in microbiome composition for both healthy and psoriasis-affected individuals. This implies that both individual-specific attributes and the specific body site contribute to the microbial diversity observed within healthy individuals (Supplementary Tables S3 and S4). The principal coordinates analysis based on Bray–Curtis distances (Supplementary Figure S4a) illustrates the dispersion of all samples, indicating high intragroup variability and dissimilarity among them. The overlap and lack of distinct group clustering in the principal coordinates analysis plot suggests that this method is less effective in discriminating between them on the basis of the species' relative abundance. Using Robust Aitchison beta-diversity (robust principal component analysis), we observed significant differences between the groups (Supplementary Figure S4b). The robust principal component analysis plot shows that lesional samples form a distinct cluster, indicating that these samples have a different microbial composition compared with those from the nonlesional, healthy top, and healthy back scalp areas.

Alpha-diversity findings within each sample group revealed a significantly ($FDR < 0.0001$) lower number of species (Chao richness observed) on lesional psoriatic scalp areas than those on healthy and nonlesional scalp areas (Supplementary Figure S5).

Altered scalp microbiota patterns in psoriasis lesions compared with those in healthy scalp: decreased

Cutibacterium and increased *Staphylococcus* abundance

For taxonomic profiling, MetaPhlAn (version 4.0) (Blanco-Míguez et al, 2023) was employed, utilizing a comprehensive reference database encompassing both metagenomic-assembled genomes and isolate references. At the kingdom level, healthy (top and back) and psoriasis capitis (nonlesional and lesional) scalps were primarily covered with bacteria, followed by fungi (Figure 4 and Supplementary Figure S6 and Supplementary Tables S5–12). Among the detected taxa, a total of 304 genera were identified across all samples; however, only a limited number of bacterial and fungal genera dominated (Supplementary Figure S6c and Supplementary Tables S9 and S10). Several of the dominant bacterial and fungal genera were typical skin commensals, including *Cutibacterium*, *Staphylococcus*, *Malassezia*, and *Corynebacterium*. *Cutibacterium* emerged as the predominant genus across the 4 groups, whereas its average relative abundance was generally lower in lesional scalp areas than in the nonlesional counterparts and healthy scalp areas. The subsequent prominent genus on the scalp was *Staphylococcus*. Its average relative abundance showed an increasing trend on psoriasis lesional scalp areas. *Malassezia*, ranked as the third most abundant genus, demonstrated an increasing average relative abundance on lesional scalp areas.

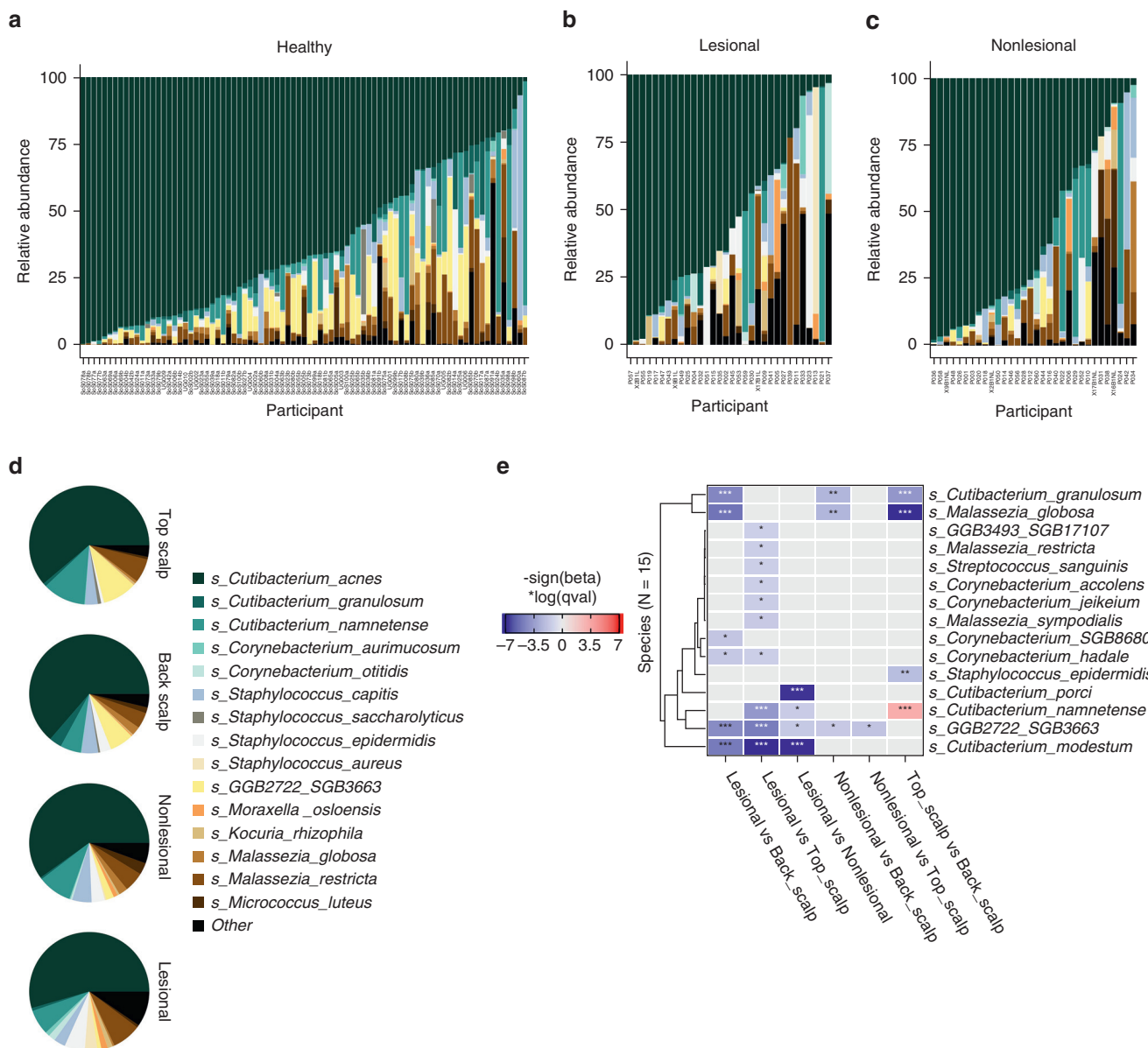


Figure 4. Relative abundance of microbial species in scalp samples from healthy individuals and individuals with psoriasis capitis. Fifteen most common kSGBs and uSGBs ordered by *Cutibacterium acnes'* relative abundance, stratified by sample group: (a) healthy individuals, (b) lesional scalp areas, and (c) nonlesional scalp areas of individuals with psoriasis. (d) Average relative abundance of top 15 species stratified by sample group: top and back scalp areas from healthy participants ($n = 43$) and nonlesional and lesional scalp areas from participants with psoriasis capitis ($n = 33$). (e) Differential microbial species ($n = 15$) in psoriasis capitis and healthy scalp areas. Representative significant species associations (FDR < 0.05) detected by MaAsLin 2.0's default linear mixed effects model ($n = 15$). All detected associations were adjusted for body site as a fixed effect and adjusted for subjectID when samples were obtained from the same participant. Values are log-transformed relative abundances. Complete linkage clustering of Pearson correlation coefficients was used to hierarchically cluster the features. Asterisks indicate the significance level of FDR-adjusted P -values: *** $P < .001$, ** $P < 0.01$, and * $P < .05$. FDR, false discovery rate; kSGB, known species-level genome bin; uSGB, uncharacterized species-level genome bin.

In total, 738 species were found across all samples, but only 15 species covered more than 90% of the scalp microbiome for each of the sample groups (Figure 4 and Supplementary Figure S6d and Supplementary Tables S11 and S12). The largest fraction of the scalp microbiome encompassed taxonomic units with available reference genomes from cultivation, known as known species-level genome bins. A smaller fraction was covered with taxa defined solely on the basis of metagenomic-assembled genomes, known as uncharacterized species-level genome

bins. *Cutibacterium acnes* appeared as the prevailing bacterial species within all 4 examined groups, whereas the lowest average relative abundance was observed in areas affected by psoriasis lesions on the scalp. The uncharacterized species-level genome bins identified as SGB3663, ranking as the third most prevalent species on both the top and back regions of the scalp, displayed a significantly higher relative abundance in healthy scalp regions than in psoriasis-affected areas (Figure 4e). This species is attributed to the genus-level genome bin 2722 within the Actinobacteria phylum and

does not yet have a sequenced isolate representative, signifying a species that is yet to be cultivated. Other notable species comprised *S. aureus*, *S. epidermidis*, *Moraxella osloensis*, *Kocuria rhizophila*, and *C. otitidis*, which exhibited a relatively higher presence on both nonlesional and lesional scalp regions than in healthy scalp areas. Although the species averages within the 4 groups suggest certain trends, the individual-stacked bar graphs reveal a substantial interindividual variability, characterized by a consistent decline in the abundance of *C. acnes* within each sample group (Figure 4a–d).

Pairwise comparisons were conducted among lesional and nonlesional areas, lesional and top scalp areas, lesional and back scalp areas, nonlesional and top scalp areas, nonlesional and back scalp areas, and top and back scalp areas (Figure 4e and Supplementary Table S13). In total, 6 pairwise comparisons revealed 15 significant taxonomic associations, where lesional scalp areas exhibited a significantly ($FDR < 0.05$) lower relative abundance of *Cutibacterium* species (including *C. modestum*, *C. namnetense*, *C. granulosum*, *C. porci*).

Microbial functional alterations in psoriatic scalps compared with those in healthy scalps

Metagenomics also facilitated the analysis of the microbial communities' collective functional potential. We used the HUMAnN pipeline (version 3.6) (Beghini et al, 2021) to estimate the relative abundances of the MetaCyc pathways for each metagenome (Supplementary Figure S7 and Supplementary Tables S14 and S15). These pathways were primarily involved in biosynthetic processes, specifically the biosynthesis of nucleosides and nucleotides; amino acids; and cofactors, carriers, and vitamins. These pathways were considered fundamental pathways because they were highly conserved, essential for basic cellular functions, and present in all samples (Supplementary Figure S7 and Supplementary Tables S14 and S15).

Using MaAsLin 2.0 (Mallick et al, 2021), a total of 120 pathways were identified as differentially abundant when combining the results of all 3 pairwise comparisons: lesional versus nonlesional, lesional versus back scalp, and lesional versus top scalp (Supplementary Figure S8 and Supplementary Table S16). No functional associations were observed between nonlesional and back scalp areas, nonlesional and top scalp areas, or top and back scalp areas. A heatmap was used to visualize the 25 pathways that were differentially abundant in all 3 pairwise comparisons (Figure 5). There was a significant ($FDR < 0.05$) increase in peptidoglycan metabolism. Other pathways that were enriched in lesional skin compared with those in nonlesional and healthy scalp areas included the superpathway of branched amino acid synthesis, pathways involved in L-isoleucine biosynthesis, and pyruvate fermentation to isobutanol. Furthermore, pathways involved in methionine metabolism were also significantly ($FDR < 0.05$) higher in lesional scalp areas than in nonlesional and healthy scalp areas (Figure 5).

The remaining 18 pathways were significantly higher in nonlesional, top scalp, and back scalp areas than in lesional scalp areas (Figure 5). Functional profiles showed significant changes in carbohydrate energy production, nucleoside and

nucleotide biosynthesis, cell structure biosynthesis, amino acid biosynthesis and amino acid degradation, carrier and vitamin biosynthesis, fatty acids and lipids biosynthesis, as well as secondary metabolite biosynthesis (Supplementary Figure S8 and Supplementary Table S16).

Virulence factor and antimicrobial resistance genes enriched in psoriatic scalp lesions

Virulence factor (VF) genes that were found on the scalp belong to different VF classes (Supplementary Figure S9). The average number of microbial reads per sample was 4.3 million reads (range: 141 million to 10.5 thousand, $n = 147$). An average of 3.91% of the quality controlled decontaminated reads were assigned to VF genes (Supplementary Figure S10a). A significantly ($FDR < 0.05$) higher proportion of VF genes was found in top and back scalp areas of healthy participants than in nonlesional scalp areas of patients with psoriasis. However, no significant differences in the proportion of VF reads to the total number of decontaminated reads were found on lesional scalp areas compared with those on nonlesional, top, and back scalp areas (Supplementary Figure S10a).

In lesional scalp areas, there was a significant increase of specific VF genes (Figure 6 and Supplementary Table S17) (MaAsLin 2.0 results). Among these genes, *VF0157*, *VF0430*, and *VF0273* all encode VF genes of flagella (involved in motility). In addition, the *VF0504* gene is related to the AdeFGH efflux pump, contributing to biofilm formation, whereas *VF0568* and *VF0451* respectively encode AcrAB and MtrCDE, associated with antimicrobial activity and competitive advantage. Compared with nonlesional, top, and back scalp areas, a significant reduction of 32 VF genes was observed in lesional scalp areas, and these genes are involved in various regulatory functions (such as *RelA* and *DevRS*), adherence (including *IlpA*), nutritional and metabolic processes (including *Shu*), immune modulation (including *PgdA*), and others. This comprehensive analysis of VF genes across various scalp areas revealed distinct patterns in healthy and psoriasis-affected subjects, highlighting the prevalence of diverse VF classes and their potential in immune modulation, stress survival, adherence, regulation, and metabolic processes.

Our study further delved into the microbial landscape by leveraging the hierarchical structure of the Comprehensive Antimicrobial Resistance Database. This allowed us to effectively categorize reads and associate them with their corresponding antimicrobial resistance (AMR) gene families and allelic variants. An average of 1.79% of the quality controlled decontaminated reads was assigned to AMR elements (Supplementary Figure S10b). Similarly, to the VF genes, we found a significantly ($FDR < 0.05$) higher proportion of AMR genes in top and back scalp areas of healthy participants than in nonlesional scalp areas of patients with psoriasis (Supplementary Figure S10b). Across all sample groups, the most common AMR genes included the adenosine triphosphate-binding cassette superfamily efflux pump, rifamycin resistance gene, the major facilitator superfamily efflux pump, the resistance nodulation division (RND) efflux pump, and additional AMR elements, as indicated in Supplementary Figure S11.

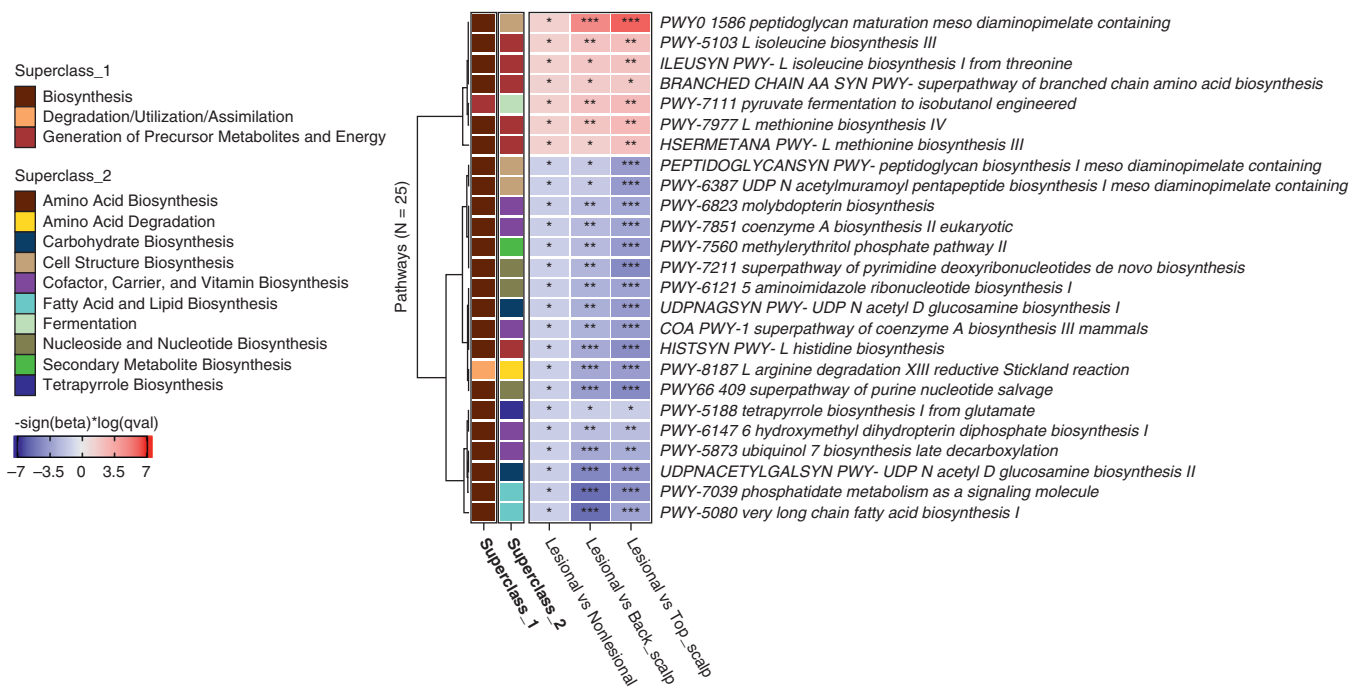


Figure 5. Functional pathways (N = 25) associated with lesional scalp areas compared with those associated with nonlesional, back, and top scalp areas.
 Representative significant pathway associations ($FDR < 0.05$) detected by MaAsLin 2.0's default linear mixed effects model. All detected associations were adjusted for body site as a fixed effect and adjusted for subjectID when samples were obtained from the same participant. Values are log-transformed relative abundances. Complete linkage clustering of Pearson correlation coefficients was used to hierarchically cluster the features. Asterisks indicate the significance level of FDR-adjusted P -values: *** $P < .001$, ** $P < .01$, and * $P < .05$. FDR, false discovery rate.

Using MaAsLin 2.0 (Mallick et al., 2021), a significant ($FDR < 0.01$) increase in the RND antibiotic efflux pump on lesional scalp areas was observed compared with that on nonlesional, top, and back scalp areas (Supplementary Figure S12 and Supplementary Table S18). Furthermore, a significant ($FDR < 0.05$) elevation of multidrug and toxic compound extrusion transporter and general bacterial porin with reduced permeability to beta-lactams was found on lesional scalp areas compared with that on top and back scalp areas of healthy participants. A significantly ($FDR < 0.05$) higher relative abundance of the major facilitator superfamily efflux pump was observed in lesional scalp areas than in top scalp areas (Supplementary Figure S12). In this manner, our investigation not only shed light on the distribution of AMR genes across diverse scalp areas but also underscored the significance of specific AMR elements in relation to both healthy participants and those afflicted with psoriasis, as highlighted through our analysis.

DISCUSSION

This study addressed the need for a deeper exploration of the residing scalp microbiome on lesional and nonlesional scalp areas of patients with psoriasis capitis as opposed to homeostatic scalp microbiota from healthy individuals. Using whole-metagenome sequencing and qPCR, we found a notable reduction in microbial load in lesional scalp areas compared with that in their nonlesional counterparts and those from healthy individuals. The increased background of human DNA; the altered microenvironment; systemic inflammation; and the presence of antimicrobial peptides

(AMPs), such as cathelicidin LL-37, in lesional scalp areas may contribute to this reduced microbial load, impacting commensal species such as *Cutibacterium* spp. in psoriatic lesions. Furthermore, this drop in microbial load was concomitant with a significant relative increase in specific virulence and AMR genes, including the MtrCDE efflux pump from the RND efflux pump family, within psoriatic scalp lesions. These efflux pumps have the potential to specifically cope with human AMPs, such as cathelicidin LL-37, potentially fostering bacterial pathogenicity and playing a role in the development of psoriasis. These pivotal findings emphasise the need for further comprehensive exploration and mode of action studies in the etiology of psoriasis capitis.

The observed significant decrease in microbiota abundance, both bacteria and fungi, on lesional scalp areas can be attributed to several factors (Figure 2 and Supplementary Figure S2). These include augmented desquamation of keratinocytes (Tett et al., 2017), resulting in an increased background of host DNA; heightened antimicrobial activity in psoriatic lesions, involving molecules such as cathelicidin LL-37, β -defensins, elafin, RNase 7, among others (Büchau and Gallo, 2007; Harder and Schröder, 2005; Lai and Gallo, 2009; Morizane and Gallo, 2012); an altered microenvironment (Dainichi et al., 2018); and increased systemic inflammation (Nestle et al., 2009). Our findings agree with those of Tett et al (2017) who found reduced microbial reads in psoriatic lesions compared with those in nonlesional skin. Similarly, our findings parallel those from Vieira-Silva et al (2019), given that psoriasis capitis is a chronic inflammatory condition. They demonstrated lowered microbial cell

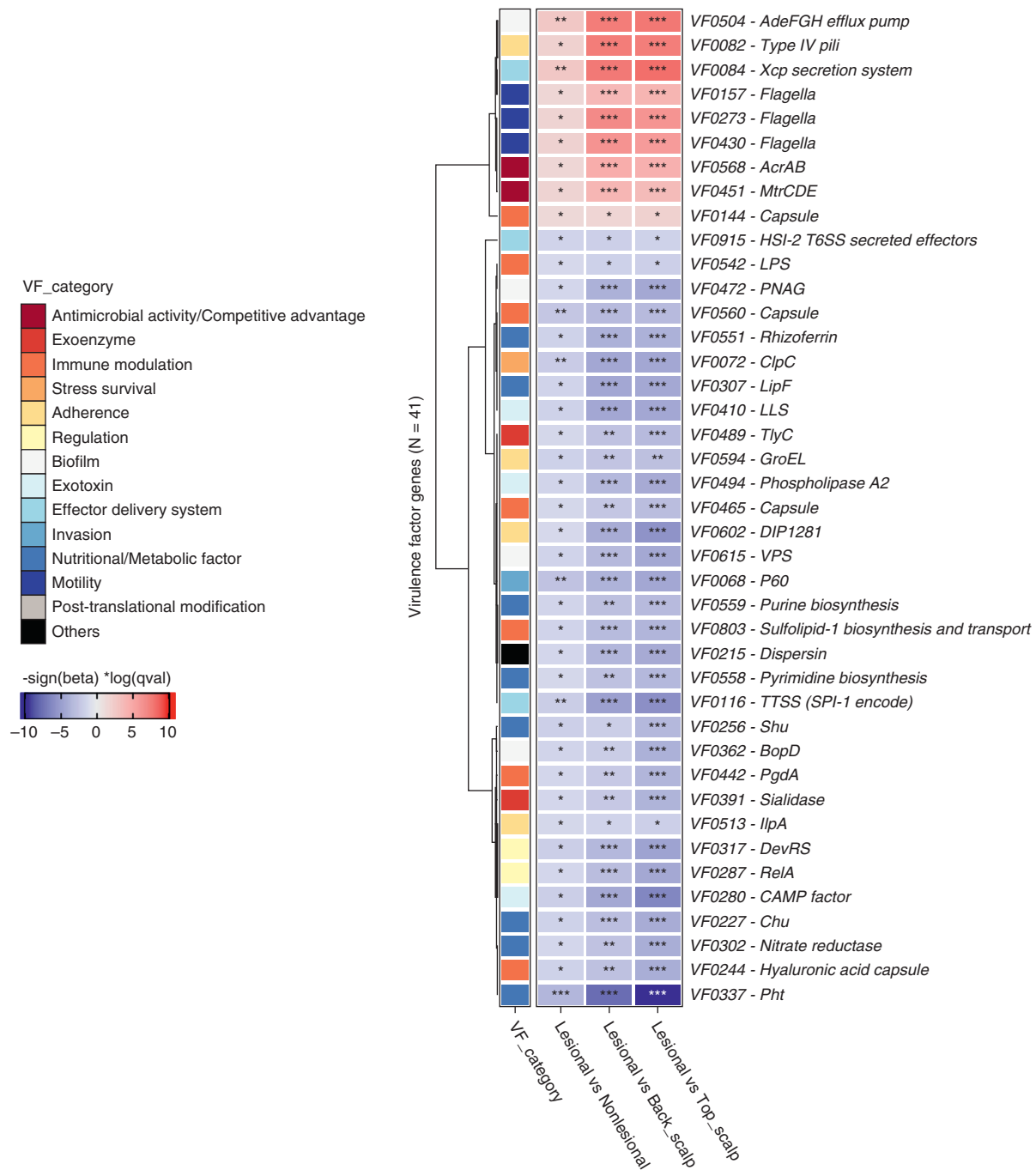


Figure 6. VF genes (N = 41) associated with lesional scalp areas compared with those associated with nonlesional, back, and top scalp areas. Representative significant VF associations (FDR < 0.05) detected by MaAsLin 2.0's default linear mixed effects model. All detected associations were adjusted for body site as a fixed effect and adjusted for subjectID when samples were obtained from the same participant. Values are log-transformed relative abundances. Complete linkage clustering of Pearson correlation coefficients was used to hierarchically cluster the features. Asterisks indicate the significance level of FDR-adjusted P-values: ***P < .001, **P < .01, and *P < .05. FDR, false discovery rate; VF, virulence factor.

counts as a key feature of dysbiosis in patients with inflammatory bowel disease and primary sclerosing cholangitis or Crohn's Disease, along with an association between reduced microbial cell counts and elevated systemic inflammation markers (Vieira-Silva et al, 2019).

In terms of microbiome diversity measures, we observed a significant decreased microbial diversity (Chao1 alpha-diversity) in the lesional scalp areas of patients with psoriasis

capitis, a pattern observed in various diseases, such as atopic dermatitis (Callewaert et al, 2020), Crohn's disease (Manichanh et al, 2006; Vieira-Silva et al, 2019), necrotizing enterocolitis (McMurtry et al, 2015), and psoriatic arthritis (Scher et al, 2015). Our observations confirm those from previous studies (Vandepitte et al, 2017; Vieira-Silva et al, 2019), where reduced species richness comes with reduced microbial load. The decreased species richness and increased

dissimilarity (Bray–Curtis) observed in psoriasis lesional scalp areas highlight the distinct microenvironments of the affected skin regions. Psoriatic lesions tend to be drier, and it is not unlikely that they harbor a microbial composition different from that of healthy and nonlesional scalp areas that tend to be sebum rich, containing several antimicrobial constituents (Drake et al, 2008; Grice and Segre, 2011; Nakatsuji et al, 2010; Wille and Kydonieus, 2003). Because psoriasis is considered an immune-mediated inflammatory condition, we can assume that the microbial signatures in the affected scalp areas may exhibit more pronounced differences than those in healthy individuals, as previously suggested (Tett et al, 2017). In our study, we observed the greatest dissimilarities in microbiota composition within the lesional scalp areas (inter-individual differences), with no significant effect of the sampled body site (lesional vs nonlesional) on the microbiome composition within patients with psoriasis (Figure 3). Systemic inflammation plays an important role in the onset and development of psoriasis (Nestle et al, 2009). Environmental or genetic triggers may induce stressed cells to initiate psoriasis pathogenesis and trigger the immune cascade, resulting in disease maintenance characterized by keratinocyte hyperproliferation and the production of β -defensins, AMPs, and chemokines (eg, IL-17, IL-22) (Nestle et al, 2009). This inflammatory microenvironment can disrupt the microbial community from its stable state, leading to a more variable and dissimilar microbiome composition in psoriasis lesions (Figure 3). This suggests a less consistent microbiome composition in lesional scalp areas among individuals with psoriasis. Furthermore, the selective pressures exerted by the inflammatory state could favor the survival and proliferation of specific microbial taxa that are more resilient to inflammation, thereby driving evolutionary changes in the microbial community structure. This suggests that intrinsic variability, local factors, and the influence of systemic inflammation associated with the condition may drive the microbial composition of individuals with psoriasis, consistent with prior studies (Human Microbiome Project Consortium, 2012; Costello et al, 2009; Oh et al, 2014). However, there are many confounding factors related to local changes (eg, skin pH, sebum levels, moisture level) that make it difficult to conclusively determine the role of systemic inflammation in these shifts.

In accordance with previous studies (Human Microbiome Project Consortium, 2012; Oh et al, 2014; Tett et al, 2017), our findings confirm the presence of a diverse community of microorganisms on the skin, both in terms of taxonomy and function. In the field of microbiome research, it is important to note that the limited number of reference genomes accessible from public databases only represents a fraction of the *in vivo* biodiversity, which is highlighted in the study of Tett et al (2017). Despite the large number of known species-level genome bins that were identified on the scalp, the taxonomic profile in this study was extended with uncharacterized species-level genome bins and genera belonging to the phylum of the Actinobacteria. Top and back scalp areas contained relatively more uncharacterized species-level genome bins than lesional and nonlesional scalp areas. This disparity may stem from a bias in researchers' cultivation eagerness because they tend to prioritize medically relevant species or the isolation of pathogens and pathology-

associated isolates. Increasing cultivation efforts and single-cell sequencing techniques should enable the characterization of these species (Byrd et al, 2018; Lasken and McLean, 2014; Scholz and Kilian, 2016). Across our cohort, the sebaceous scalp environment was dominated by *Cutibacterium* species and demonstrated a low species diversity, as seen in earlier studies (Byrd et al, 2018; Scholz and Kilian, 2016). Although *C. acnes* is a dominant species on the scalp, our findings demonstrate that it is not significantly altered, although a general decrease was observed on lesional scalp areas (Figure 4d). We observed a significant decrease in several minor *Cutibacterium* spp., including *C. modestum*, *C. namnetense*, *C. granulosum*, and *C. porci*, in lesional scalp areas compared with those in healthy and nonlesional scalp areas (Figure 4e), suggesting their important role as skin commensals. The relative abundance of *S. aureus* was on average higher (Figure 4d and Supplementary Figure S6) in lesional scalp areas, consistent with previous psoriasis studies (Gao et al, 2008; Tett et al, 2017). These results suggest *S. aureus*' potential involvement in psoriasis pathogenesis. We also observed a significant reduction in various *Corynebacterium* and *Malassezia* species in lesional scalp areas compared with those in healthy regions (Figure 4e). This could likely be due to lipid auxotrophy, a characteristic shared by skin-resident microorganisms (Byrd et al, 2018; Swaney et al, 2023). These genera, including *Cutibacterium*, rely on external sources of fatty acids for their growth and metabolism (Bojar and Holland, 2002; Bouslimani et al, 2015; Byrd et al, 2018; Tauch et al, 2005). This dependence may explain the reduced presence of these species on dry, lesional scalp areas compared with that on sebum-rich, healthy scalp regions. These results indicate that changes in the microenvironment of psoriatic lesions, such as sebum loss, may significantly affect the microbial composition and dynamics of the scalp ecosystem.

The scalp areas affected by psoriasis lesions exhibited significant alterations in microbial metabolic pathways ($N = 120$) in comparison with the nonlesional, top, and back scalp regions (Figure 5 and Supplementary Figure S8). These alterations can disrupt skin homeostasis, activating keratinocytes and immune cells (Chen et al, 2018). Pathways related to gondoate biosynthesis (anaerobic) and cytidine diphosphate-diacylglycerol biosynthesis were significantly enriched in psoriatic scalp lesions compared with those in healthy scalp regions (top and back). Similar observations have been obtained from patients with allergic rhinoconjunctivitis and allergic rhinitis (Wang et al, 2023). The glyoxylate bypass glyoxylate cycle, known to be upregulated in response to oxidative stress (Ahn et al, 2016), was also significantly ($FDR < 0.05$) enriched, suggesting its potential involvement in psoriasis development. Psoriasis is thought to be a chronic autoimmune condition initiated by allergic reactions and shows strong indications of oxidative stress: altered antioxidant enzymes, oxidized proteins, and oxidized lipids (Bayer et al, 2005; Dimon-Gadal et al, 2000; Kadam et al, 2010; Yazici et al, 2016). Furthermore, ethanolamine utilization, associated with bacterial pathogenesis (Garsin, 2010), showed significant ($FDR < 0.05$) enrichment in psoriatic scalp areas compared with that in healthy regions. In addition, this study found significantly ($FDR < 0.05$) elevated

pathways related to methionine production in psoriatic skin lesions compared with that in healthy and nonlesional skin. The study of Ruseva et al (2021) demonstrated a significant increase in methionine levels within psoriatic plaques, when compared with that in unaffected skin of patients with psoriasis. This indicates that alterations in microbial methionine metabolism could have a significant impact on the development of psoriasis because methionine serves as the exclusive supplier of propylamine groups needed for polyamine synthesis (Ruseva et al, 2021). In addition, methionine plays a crucial role in methylation processes, the generation of homocysteine, and the synthesis of glutathione (Ruseva et al, 2021).

VF and AMR genes that were enriched in lesional scalp areas play crucial roles in the pathogenicity of microbiota and their ability to cause infections or exacerbate conditions. In this study, 3 of the 5 families of efflux pump proteins associated with multidrug (antibiotic) resistance were found to be significantly enriched in lesional scalp areas compared with those in nonaffected scalp areas (Piddock, 2006). These enriched families included the RND antibiotic efflux pump, multidrug and toxic compound extrusion transporter, and major facilitator superfamily antibiotic efflux pump (Supplementary Figure S12).

AcrAB and MtrCDE, both belonging to the efflux pumps of the RND family, play a role in antimicrobial activity and competitive advantage (Piddock, 2006). RND efflux pumps have been associated with bacterial colonization and survival in the host. These pumps are known for multidrug resistance and may also transport VFs (including adhesins, toxins, among others), influencing host colonization and infection. AcrAB aids in removing toxic compounds, including antibiotics, from bacteria (Ma et al, 1993), whereas MtrCDE is linked to multidrug resistance and antimicrobial agent efflux. The enrichment of the MtrCDE efflux pump in psoriatic lesional areas may confer resistance to AMPs, including human LL-37 (also known as cathelicidin AMPs). Research by Shafer et al (1998) demonstrated that endogenous AMPs, including protegrin-1 and human LL-37, are substrates of the MtrCDE efflux pump in certain bacteria, potentially allowing microorganisms to evade LL-37's effects and persist in psoriatic lesions. In lesional scalp areas, the elevated presence of these efflux pumps may contribute to antibiotic resistance, allowing certain microorganisms to dominate and potentially alter microbial community composition. This alteration could contribute to psoriatic scalp conditions and render current therapeutic approaches ineffective in curing the scalp lesions.

Furthermore, this study revealed a significant increase in the relative abundance of the AdeFGH efflux pump in lesional scalp areas, which is involved in biofilm formation. According to previous studies, this VF gene may play a role in the production and translocation of chemical signaling molecules (autoinducers) during biofilm infections in chronic wounds (He et al, 2015). In addition, a significant increase of type IV pili was detected in lesional scalp areas. These dynamic filaments exhibit rapid polymerization and depolymerization, enabling them to perform a wide range of functions, including acquiring genes, exhibiting twitching motility, and forming microcolonies (Craig et al, 2019). The mechanisms through which these VF genes influence

inflammatory skin conditions could provide a deeper insight into psoriasis capitis pathogenesis. However, our findings are preliminary and require further validation through future experiments.

Although metagenomic sequencing revealed functional properties, virulome, and resistome genes, future transcriptomic, proteomic, and/or metabolomic analyses are required to further confirm the altered microbiome functionality in lesional and/or nonlesional skin sites of patients with psoriasis. These additional analyses could entail the incorporation of skin biophysical measurements, such as skin sebum level and skin surface AMPs as well as an assessment of the inflammation markers at the serum level and, in view of the further insights into the hypothesized gut–skin axis (De Pessemier et al, 2021; Dokoshi et al, 2024; O'Neill et al, 2016), a correlation analysis with the participants' gut health and microbiome. These additional considerations would contribute to a more comprehensive understanding of psoriasis capitis and its link to the gut. Efforts to uncover the functional impact of microbial dysbiosis in the skin may also support an increased understanding of how the effects extend beyond the skin. Differential diagnosis of psoriasis from other scalp disorders, for example, seborrheic dermatitis and sebopsoriasis, is important owing to their overlapping yet distinct lesions and the effectiveness of the appropriate therapeutic treatments. Our findings shed light on the complex dynamics at play in psoriasis capitis lesional scalp areas and may have significant implications for future research and clinical approaches in this field.

MATERIALS AND METHODS

Study design

The scalp microbiome was mapped for both healthy subjects (top and back scalp areas) and subjects with untreated psoriasis capitis (lesional and nonlesional scalp areas) (Figure 1 and Supplementary Table S1). Exclusion criteria included age <18 years, pregnancy, and topical or antibiotic usage in the preceding 3 months (Dréno et al, 2016). Patients with psoriasis who suffered from any other skin condition were excluded from the study. This study and all experiments were implemented in accordance with the ethical principles and regulations of the medical ethics committee of University Hospital Ghent, Ghent University and AZ Delta (B670201941161). All participants were fully informed of the procedure and purpose of the study and gave their written informed consent. A total of 76 subjects consented to participate (Supplementary Tables S1 and S2). Among these participants, 43 were chosen as healthy test subjects after confirming the health of their scalp through a brief survey. In addition, 33 patients diagnosed with untreated psoriasis capitis were recruited from the Dermatology Research Unit at Ghent University Hospital ($n = 12$) and AZ Delta Roeselare ($n = 21$) for inclusion in the study. Differentiation from other scalp disorders (eg, seborrheic dermatitis and sebopsoriasis) was based on the appearance of scales, well-defined erythematous (redness) plaques, and the distribution of psoriasis lesions on other parts of the body. Associated metadata were collected from both healthy individuals and those with psoriasis, including biological sex, age, anthropometrics (weight, length, body mass index), ethnicity, diet, weekly alcohol intake, smoking patterns, profession, physical activity, and skin condition (Supplementary Table S2).

Sample collection and DNA extraction

We sampled a standardized $\pm 100 \text{ cm}^2$ ($10 \times 10 \text{ cm}$) area of the top and the back of the scalp (healthy participants) or lesional and nonlesional scalp area (participants with untreated psoriasis capitis) for 30 seconds. This approach aimed to minimize variation associated with geographical location (Alekseyenko et al, 2013; Fahlén et al, 2012; Gao et al, 2008). A sterile cotton swab (Biolab ZRT) was immersed in a sterile normal saline solution (8.5 g sodium chloride per liter). The swab was stored in a sterile DNase-RNase-free tube without normal saline solution at -20°C . The sampling of the patients with psoriasis capitis in the 2 hospitals was carried out analogously by the on-site dermatologists. The samples were stored on site at -20°C and subsequently stored at the Center for Microbial Ecology and Technology at -20°C until further analyses.

The DNA of most samples was extracted using the DNeasy PowerSoil Pro Kit (Qiagen) according to the manufacturer's instructions (Supplementary Table S2). A separate approach was adopted for the first 14 samples. These 14 samples underwent DNA extraction through a combination of chemical and mechanical lysis as described by Geirnaert et al (2015) (Supplementary Table S2). However, this approach proved ineffective for the remaining samples owing to their low biomass.

qPCR analysis

The abundances of bacteria were quantitatively determined in all psoriasis samples by real-time PCR targeting the bacterial V3–V4 region of the 16S rRNA gene using the universal primers 338F (ACTCCTACGGGAGGCAGCAC) and 518R (ATTACCGCGGTGCTGG) (Orschler et al, 2019). The fungal load of each sample was determined targeting 18S rRNA gene using the FungiQuant forward (GGRAAACTCACCAGGTCCAG) and FungiQuant reverse (GSWCTATCCCCAKCACGA) primers and FungiQuant P (TGGTGCATGGCCGTT) probe (Liu et al, 2012). To normalize the bacterial and fungal load, the human load of each sample was determined by targeting the ACTB gene using the ACTB forward (CTGGAACGGT-GAAGGTGACA) and ACTB reverse (AAGGGACTTCCTGTAA-CAATGCA) primers (Li et al, 2011). The protocols are detailed in Supplementary Materials and Methods.

Whole-genome shotgun sequencing, data processing, and statistical data analysis

DNA libraries were prepared using the Nextera XT DNA Library Preparation Kit (Illumina) and IDT Unique Dual Indexes with a total DNA input of 1 ng. Genomic DNA was fragmented using a proportional amount of Illumina Nextera XT fragmentation enzyme. Unique dual indexes were added to each sample, followed by 15 cycles of PCR to construct libraries. DNA libraries were purified using AMPure magnetic beads (Beckman Coulter) and eluted in Qiagen EB buffer. DNA libraries were quantified using a Qubit 4 fluorometer (Supplementary Table S2) and Qubit dsDNA HS Assay Kit. Libraries were then sequenced on an Illumina NovaSeq S4 platform $2 \times 150 \text{ bp}$.

The generated raw metagenomes were processed through the Biobakery pipeline (Beghini et al, 2021), and the statistical data analyses were performed as detailed in Supplementary Materials and Methods.

ETHICS STATEMENT

This study and all experiments were implemented in accordance with the ethical principles and regulations of the medical ethics committee of University Hospital Ghent, Ghent University and AZ Delta (B670201941161). Before participating in this study, all volunteers were fully informed of the

procedure and purpose of the study and gave their written informed consent. A total of 76 subjects consented to participate (Supplementary Tables S1 and S2).

DATA AVAILABILITY STATEMENT

All data generated or analyzed during this study are included in this published article and its supplementary materials. The datasets generated during this study are available in the European Nucleotide Archive at EMBL-European Bioinformatics Institute under accession number PRJEB67362 (<https://www.ebi.ac.uk/ena/browser/view/PRJEB67362>). The codebase and datasets that were used to analyze the data are available in the following GitHub repository: https://github.com/bdpessem/PsoriasisCapitis_WMS.git.

ORCIDs

Britta De Pessemier: <http://orcid.org/0000-0002-3249-176X>
 Celia Díez López: <http://orcid.org/0000-0001-8201-1157>
 Steff Taelman: <http://orcid.org/0000-0002-2685-4130>
 Merel Verdonck: <http://orcid.org/0009-0007-2310-5090>
 Yang Chen: <http://orcid.org/0000-0002-0164-8971>
 Annelies Stockman: <http://orcid.org/0000-0003-1203-8076>
 Jo Lambert: <http://orcid.org/0000-0001-5303-9310>
 Tom Van de Wiele: <http://orcid.org/0000-0001-6854-5689>
 Chris Callewaert: <http://orcid.org/0000-0001-7697-9188>

CONFLICT OF INTEREST

The authors state no conflict of interest.

ACKNOWLEDGMENTS

BDP was supported by the Research Foundation Flanders (grant number 1S04122N). CC was supported by the Research Foundation Flanders (FWO19/PDS/084). ST was supported by the Vlaams Agentschap Innoveren en Ondernemen (HBC.2020.2292).

AUTHOR CONTRIBUTIONS

Conceptualization: BDP, CC, TVdW; Data Curation: BDP, CC; Formal Analysis: BDP, CC, CDL, ST; Funding Acquisition: BDP, CC, TVdW; Investigation: BDP, MV, JL, AS; Methodology: BDP, CC; Project Administration: BDP, CC; Resources: BDP, CC, CDL, ST, JL, AS, YC, TVdW; Software: BDP, ST; Supervision: CC, TVdW; Validation: BDP; Visualization: BDP, CDL; Writing - Original Draft Preparation: BDP; Writing - Review and Editing: BDP, CC, CDL, ST, JL, AS, YC, TVdW, MV

SUPPLEMENTARY MATERIAL

Supplementary material is linked to the online version of the paper at www.jidonline.org, and at <https://doi.org/10.1016/j.jid.2024.07.020>.

REFERENCES

- Ahn S, Jung J, Jang IA, Madsen EL, Park W. Role of glyoxylate shunt in oxidative stress response. *J Biol Chem* 2016;291:11928–38.
- Ainali C, Valeev N, Perera G, Williams A, Gudjonsson JE, Ouzounis CA, et al. Transcriptome classification reveals molecular subtypes in psoriasis. *BMC Genomics* 2012;13:472.
- Alekseyenko AV, Perez-Perez GI, De Souza A, Strober B, Gao Z, Bihan M, et al. Community differentiation of the cutaneous microbiota in psoriasis. *Microbiome* 2013;1:31.
- Armstrong AW, Mehta MD, Schupp CW, Gondo GC, Bell SJ, Griffiths CEM. Psoriasis prevalence in adults in the United States. *JAMA Dermatol* 2021;157:940–6.
- Armstrong AW, Read C. Pathophysiology, clinical presentation, and treatment of psoriasis: a review. *JAMA* 2020;323:1945–60.
- Aßhauer KP, Wemheuer B, Daniel R, Meinicke P. Tax4Fun: predicting functional profiles from metagenomic 16S rRNA data. *Bioinformatics* 2015;31: 2882–4.
- Bayer M, Mosandl A, Thaci D. Improved enantioselective analysis of polyunsaturated hydroxy fatty acids in psoriatic skin scales using high-performance liquid chromatography. *J Chromatogr B Anal Technol Biomed Life Sci* 2005;819:323–8.
- Beghini F, McIver LJ, Blanco-Míguez A, Dubois L, Asnicar F, Maharjan S, et al. Integrating taxonomic, functional, and strain-level profiling of diverse microbial communities with bioBakery 3. *eLife* 2021;10:e65088.
- Blanco-Míguez A, Beghini F, Cumbo F, McIver LJ, Thompson KN, Zolfo M, et al. Extending and improving metagenomic taxonomic profiling with

- uncharacterized species using MetaPhlAn 4. *Nat Biotechnol* 2023;41:1633–44.
- Boehncke WH, Schön MP. Psoriasis. *Lancet* 2015;386:983–94.
- Bojar RA, Holland KT. Review: the human cutaneous microflora and factors controlling colonisation. *World J Microbiol Biotechnol* 2002;18:889–903.
- Bouslimani A, Porto C, Rath CM, Wang M, Guo Y, Gonzalez A, et al. Molecular cartography of the human skin surface in 3D. *Proc Natl Acad Sci U S A* 2015;112:E2120–9.
- Büchau AS, Gallo RL. Innate immunity and antimicrobial defense systems in psoriasis. *Clin Dermatol* 2007;25:616–24.
- Byrd AL, Belkaid Y, Segre JA. The human skin microbiome. *Nat Rev Microbiol* 2018;16:143–55.
- Callewaert C, Nakatsuji T, Knight R, Kosciolek T, Vrbanac A, Kotol P, et al. IL-4R α blockade by dupilumab decreases *Staphylococcus aureus* colonization and increases microbial diversity in atopic dermatitis. *J Invest Dermatol* 2020;140:191–202.e7.
- Chen YE, Fischbach MA, Belkaid Y. Skin microbiota-host interactions [published correction appears in *Nature* 2018;555:543]. *Nature* 2018;553:427–36.
- Choi JY, Kim H, Koo HY, You J, Yu DS, Lee YB, et al. Severe scalp psoriasis microbiome has increased biodiversity and relative abundance of *pseudomonas* compared to mild scalp psoriasis. *J Clin Med* 2022;11:7133.
- Costello EK, Lauber CL, Hamady M, Fierer N, Gordon JI, Knight R. Bacterial community variation in human body habitats across space and time. *Science* 2009;326:1694–7.
- Craig L, Forest KT, Maier B. Type IV pili: dynamics, biophysics and functional consequences. *Nat Rev Microbiol* 2019;17:429–40.
- Dainichi T, Kitoh A, Otsuka A, Nakajima S, Nomura T, Kaplan DH, et al. The epithelial immune microenvironment (EIME) in atopic dermatitis and psoriasis. *Nat Immunol* 2018;19:1286–98.
- De Pessemeir B, Grine L, Debaere M, Maes A, Paetzold B, Callewaert C. Gut-skin axis: current knowledge of the interrelationship between microbial dysbiosis and skin conditions. *Microorganisms* 2021;9:353.
- Dessinioti C, Katsambas A. Seborrheic dermatitis: etiology, risk factors, and treatments: facts and controversies. *Clin Dermatol* 2013;31:343–51.
- Dimon-Gadal S, Gerbaud P, Théron P, Guibourdenche J, Anderson WB, Evain-Brion D, et al. Increased oxidative damage to fibroblasts in skin with and without lesions in psoriasis. *J Invest Dermatol* 2000;114:984–9.
- Dokoshi T, Chen Y, Cavagnero KJ, Rahman G, Hakim D, Brinton S, et al. Dermal injury drives a skin to gut axis that disrupts the intestinal microbiome and intestinal immune homeostasis in mice. *Nat Commun* 2024;15:3009.
- Drake DR, Brogden KA, Dawson DV, Wertz PW. Thematic review series: skin lipids. Antimicrobial lipids at the skin surface. *J Lipid Res* 2008;49:4–11.
- Dréno B, Araviiskaia E, Berardesca E, Gontijo G, Sanchez Viera M, Xiang LF, et al. Microbiome in healthy skin, update for dermatologists. *J Eur Acad Dermatol Venereol* 2016;30:2038–47.
- Eisenstein M. The skin microbiome and its relationship with the human body explained. *Nature* 2020;588:S210–1.
- Fahlén A, Engstrand L, Baker BS, Powles A, Fry L. Comparison of bacterial microbiota in skin biopsies from normal and psoriatic skin. *Arch Dermatol Res* 2012;304:15–22.
- Gao Z, Tseng CH, Strober BE, Pei Z, Blaser MJ. Substantial alterations of the cutaneous bacterial biota in psoriatic lesions. *PLoS One* 2008;3:e2719.
- Garsin DA. Ethanolamine utilization in bacterial pathogens: roles and regulation. *Nat Rev Microbiol* 2010;8:290–5.
- Geirnaert A, Wang J, Tinck M, Steyaert A, Van den Abbeele P, Eeckhaut V, et al. Interindividual differences in response to treatment with butyrate-producing *Butyrivibrio pullicaecorum* 25-3T studied in an in vitro gut model. *FEMS Microbiol Ecol* 2015;91:fiv054.
- George SM, Taylor MR, Farrant PB. Psoriatic alopecia. *Clin Exp Dermatol* 2015;40:717–21.
- Greb JE, Goldminz AM, Elder JT, Lebwohl MG, Gladman DD, Wu JJ, et al. Psoriasis. *Nat Rev Dis Primers* 2016;2:16082.
- Grice EA, Kong HH, Conlan S, Deming CB, Davis J, Young AC, et al. Topographical and temporal diversity of the human skin microbiome. *Science* 2009;324:1190–2.
- Grice EA, Segre JA. The skin microbiome [published correction appears in *Nat Rev Microbiol* 2011;9:626]. *Nat Rev Microbiol* 2011;9:244–53.
- Harder J, Schröder JM. Psoriatic scales: a promising source for the isolation of human skin-derived antimicrobial proteins. *J Leukoc Biol* 2005;77:476–86.
- He X, Lu F, Yuan F, Jiang D, Zhao P, Zhu J, et al. Biofilm formation caused by clinical *Acinetobacter baumannii* isolates is associated with overexpression of the AdeFGH efflux pump. *Antimicrob Agents Chemother* 2015;59:4817–25.
- Hjuler KF, Iversen L, Rasmussen MK, Kofoed K, Skov L, Zachariae C. Localization of treatment-resistant areas in patients with psoriasis on biologics. *Br J Dermatol* 2019;181:332–7.
- Human Microbiome Project Consortium. Structure, function and diversity of the healthy human microbiome. *Nature* 2012;486:207–14.
- Johnson JS, Spakowicz DJ, Hong BY, Petersen LM, Demkowicz P, Chen L, et al. Evaluation of 16S rRNA gene sequencing for species and strain-level microbiome analysis. *Nat Commun* 2019;10:5029.
- Kadam DP, Suryakar AN, Ankush RD, Kadam CY, Deshpande KH. Role of oxidative stress in various stages of psoriasis. *Indian J Clin Biochem* 2010;25:388–92.
- Kim KS, Shin MK, Ahn JJ, Haw CR, Park HK. A comparative study of hair shafts in scalp psoriasis and seborrheic dermatitis using atomic force microscopy. *Skin Res Technol* 2013;19:e60–4.
- Lai Y, Gallo RL. AMPed up immunity: how antimicrobial peptides have multiple roles in immune defense. *Trends Immunol* 2009;30:131–41.
- Langille MG, Zaneveld J, Caporaso JG, McDonald D, Knights D, Reyes JA, et al. Predictive functional profiling of microbial communities using 16S rRNA marker gene sequences. *Nat Biotechnol* 2013;31:814–21.
- Lasken RS, McLean JS. Recent advances in genomic DNA sequencing of microbial species from single cells. *Nat Rev Genet* 2014;15:577–84.
- Lebwohl M. Psoriasis. *Lancet* 2003;361:1197–204.
- Li L, Yan Y, Xu H, Qu T, Wang B. Selection of reference genes for gene expression studies in ultraviolet B-irradiated human skin fibroblasts using quantitative real-time PCR. *BMC Mol Biol* 2011;12:8.
- Liu CM, Kachur S, Dwan MG, Abraham AG, Aziz M, Hsueh PR, et al. Fun-giQuant: a broad-coverage fungal quantitative real-time PCR assay. *BMC Microbiol* 2012;12:255.
- Ma D, Cook DN, Alberti M, Pon NG, Nikaido H, Hearst JE. Molecular cloning and characterization of acrA and acrE genes of *Escherichia coli*. *J Bacteriol* 1993;175:6299–313.
- Mallick H, Rahnavard A, McIver LJ, Ma S, Zhang Y, Nguyen LH, et al. Multivariable association discovery in population-scale meta-omics studies. *PLoS Comput Biol* 2021;17:e1009442.
- Manichanh C, Rigottier-Gois L, Bonnaffon E, Gloux K, Pelletier E, Frangeul L, et al. Reduced diversity of faecal microbiota in Crohn's disease revealed by a metagenomic approach. *Gut* 2006;55:205–11.
- McMurtry VE, Gupta RW, Tran L, Blanchard EE 4th, Penn D, Taylor CM, et al. Bacterial diversity and Clostridia abundance decrease with increasing severity of necrotizing enterocolitis. *Microbiome* 2015;3:11.
- Morizane S, Gallo RL. Antimicrobial peptides in the pathogenesis of psoriasis. *J Dermatol* 2012;39:225–30.
- Nakatsuji T, Kao MC, Zhang L, Zouboulis CC, Gallo RL, Huang CM. Sebum free fatty acids enhance the innate immune defense of human sebocytes by upregulating beta-defensin-2 expression. *J Invest Dermatol* 2010;130:985–94.
- Nestle FO, Kaplan DH, Barker J. Psoriasis. *N Engl J Med* 2009;361:496–509.
- Oh J, Byrd AL, Deming C, Conlan S, , NISC Comparative Sequencing Program, Kong HH, et al. Biogeography and individuality shape function in the human skin metagenome. *Nature* 2014;514:59–64.
- O'Neill CA, Monteleone G, McLaughlin JT, Paus R. The gut-skin axis in health and disease: a paradigm with therapeutic implications. *BioEssays* 2016;38:1167–76.
- Orschler L, Agrawal S, Lackner S. On resolving ambiguities in microbial community analysis of partial nitritation anammox reactors. *Sci Rep* 2019;9:6954.
- Ortonne J, Chimenti S, Luger T, Puig L, Reid F, Trüb R. Scalp psoriasis: European consensus on grading and treatment algorithm. *J Eur Acad Dermatol Venereol* 2009;23:1435–44.

- Papp K, Berth-Jones J, Kragballe K, Wozel G, de La Brassine M. Scalp psoriasis: a review of current topical treatment options. *J Eur Acad Dermatol Venereol* 2007;21:1151–60.
- Parisi R, Symmons DP, Griffiths CE, Ashcroft DM, Identification and Management of Psoriasis and Associated Comorbidity (IMPACT) project team. Global epidemiology of psoriasis: a systematic review of incidence and prevalence. *J Invest Dermatol* 2013;133:377–85.
- Paulino LC, Tseng CH, Strober BE, Blaser MJ. Molecular analysis of fungal microbiota in samples from healthy human skin and psoriatic lesions. *J Clin Microbiol* 2006;44:2933–41.
- Piddock LJ. Multidrug-resistance efflux pumps - not just for resistance. *Nat Rev Microbiol* 2006;4:629–36.
- Raza N, Usman M, Hameed A. Chronic plaque psoriasis: streptococcus pyogenes throat carriage rate and therapeutic response to oral antibiotics in comparison with oral methotrexate. *J Coll Physicians Surg Pak* 2007;17:717–20.
- Rudramurthy SM, Honnavar P, Chakrabarti A, Dogra S, Singh P, Handa S. Association of Malassezia species with psoriatic lesions. *Mycoses* 2014;57:483–8.
- Ruseva S, Popova I, Lozanov V, Mitev V. Insight into the metabolite pattern of psoriasis: correlation among homocysteine, methionine, and polyamines. *Symmetry* 2021;13:606.
- Scher JU, Ubeda C, Artacho A, Attur M, Isaac S, Reddy SM, et al. Decreased bacterial diversity characterizes the altered gut microbiota in patients with psoriatic arthritis, resembling dysbiosis in inflammatory bowel disease. *Arthritis Rheumatol* 2015;67:128–39.
- Scholz CFP, Kilian M. The natural history of cutaneous propionibacteria, and reclassification of selected species within the genus Propionibacterium to the proposed novel genera Acidipropionibacterium gen. nov., Cutibacterium gen. nov. and Pseudopropionibacterium gen. nov. *Int J Syst Evol Microbiol* 2016;66:4422–32.
- Shaffer WM, Qu X, Waring AJ, Lehrer RI. Modulation of Neisseria gonorrhoeae susceptibility to vertebrate antibacterial peptides due to a member of the resistance/nodulation/division efflux pump family. *Proc Natl Acad Sci U S A* 1998;95:1829–33.
- Skowron K, Bauza-Kaszewska J, Kraszewska Z, Wiktorczyk-Kapischke N, Grudlewska-Buda K, Kwiecińska-Pirog J, et al. Human skin microbiome: impact of intrinsic and extrinsic factors on skin microbiota. *Microorganisms* 2021;9:543.
- Swaney MH, Nelsen A, Sandstrom S, Kalan LR. Sweat and sebum preferences of the human skin microbiota. *Microbiol Spectr* 2023;11:e0418022.
- Takemoto A, Cho O, Morohoshi Y, Sugita T, Muto M. Molecular characterization of the skin fungal microbiome in patients with psoriasis. *J Dermatol* 2015;42:166–70.
- Tauch A, Kaiser O, Hain T, Goessmann A, Weisshaar B, Albersmeier A, et al. Complete genome sequence and analysis of the multiresistant nosocomial pathogen *Corynebacterium jeikeium* K411, a lipid-requiring bacterium of the human skin flora. *J Bacteriol* 2005;187:4671–82.
- Tett A, Pasolli E, Farina S, Truong DT, Asnicar F, Zolfo M, et al. Unexplored diversity and strain-level structure of the skin microbiome associated with psoriasis. *NPJ Biofilms Microbiomes* 2017;3:14.
- Tomi NS, Kränke B, Aberer E. Staphylococcal toxins in patients with psoriasis, atopic dermatitis, and erythroderma, and in healthy control subjects. *J Am Acad Dermatol* 2005;53:67–72.
- Turnbaugh PJ, Ley RE, Hamady M, Fraser-Liggett CM, Knight R, Gordon JI. The human microbiome project. *Nature* 2007;449:804–10.
- van de Kerkhof PC, Franssen ME. Psoriasis of the scalp, Diagnosis and management. *Am J Clin Dermatol* 2001;2:159–65.
- Vandepitte D, Kathagen G, D'hoe K, Vieira-Silva S, Valles-Colomer M, Sabino J, et al. Quantitative microbiome profiling links gut community variation to microbial load. *Nature* 2017;551:507–11.
- Vieira-Silva S, Sabino J, Valles-Colomer M, Falony G, Kathagen G, Caenepeel C, et al. Quantitative microbiome profiling disentangles inflammation- and bile duct obstruction-associated microbiota alterations across PSC/IBD diagnoses. *Nat Microbiol* 2019;4:1826–31.
- Wang Y, Li X, Gu S, Fu J. Characterization of dysbiosis of the conjunctival microbiome and nasal microbiome associated with allergic rhinoconjunctivitis and allergic rhinitis. *Front Immunol* 2023;14:1079154.
- Wille JJ, Kydonieus A. Palmitoleic acid isomer (C16:1delta6) in human skin sebum is effective against gram-positive bacteria. *Skin Pharmacol Appl Skin Physiol* 2003;16:176–87.
- Yazici C, Köse K, Utaş S, Tanrikulu E, Taşlidere N. A novel approach in psoriasis: first usage of known protein oxidation markers to prove oxidative stress. *Arch Dermatol Res* 2016;308:207–12.



This work is licensed under a Creative Commons Attribution-NonCommercial-NoDerivatives 4.0 International License. To view a copy of this license, visit <http://creativecommons.org/licenses/by-nc-nd/4.0/>

SUPPLEMENTARY MATERIALS AND METHODS

qPCR analysis

qPCR assays targeting the 16S ribosomal RNA gene were performed using a StepOnePlus real-time PCR system. Reactions were performed in a volume of 20 µl consisting of 10.0 µl of 2× iTaq universal SYBR Green supermix (Bio-Rad Laboratories), 2.0 µl DNA template, 0.8 µl (10 µM stock) of each primer, and 6.4 µl nuclease-free water. Amplifications were run as follows: initial denaturation for 2 minutes at 95 °C followed by 40 cycles of 15-second denaturation at 95 °C and combined annealing/extension 1' at 60 °C. At the end of the qPCR run, a melting curve analysis was performed to confirm product specificity (60–95 °C, ΔT per 15 second = 0.3 °C). Quantification was performed using a standard curve on the basis of known concentrations of DNA standard dilutions from 10⁸ copies µl⁻¹ down to 10² copies µl⁻¹. All qPCR analyses were conducted in triplicate.

qPCR assays targeting the 18S ribosomal RNA gene were performed using the QuantStudio 3 Real-Time PCR Instrument (Applied Biosystems). Reactions were performed in a volume of 20 µl consisting 2× TaqPath BactoPure Microbial Detection Master Mix (Thermo Fischer Scientific), 2.0 µl DNA template, 0.5 µl TaqMan probe (10 µM stock), 3.6 µl (10 µM stock) of each primer, and 0.3 µl nuclease-free water. Amplifications were run as follows: initial denaturation for 30 seconds at 98 °C followed by 33 cycles of denaturation for 10 seconds at 98 °C, annealing for 10 seconds at 60 °C, extension for 1 minute at 72 °C, and a final extension for 5 minutes at 72 °C. Quantification was performed using a standard curve on the basis of known concentrations of DNA standard dilutions from 10⁸ copies µl⁻¹ down to 10² copies µl⁻¹. All qPCR analyses were conducted in triplicate.

qPCR assays targeting the ACTB gene were performed using the QuantStudio 3 Real-Time PCR Instrument (Applied Biosystems). Reactions were performed in a volume of 20 µl consisting 2× PowerTrack SYBR Green MasterMix (Thermo Fischer Scientific), 2.0 µl DNA template, 0.8 µl (10 µM stock) of each primer, and 6.4 µl nuclease-free water. Amplifications were run as follows: initial denaturation for 30 seconds at 98 °C followed by 30 cycles of denaturation for 10 seconds at 98 °C, annealing for 10 seconds at 60 °C, extension for 1 minute at 72 °C, and a final extension for 5 minutes at 72 °C. Quantification was performed using a standard curve on the basis of known concentrations of DNA standard dilutions from 10⁷ copies µl⁻¹ down to 10¹ copies µl⁻¹. All qPCR analyses were conducted in triplicate.

Data processing and bioinformatics analysis

Sample quality control and subsampling. The generated raw metagenomes were processed with KneadData (Beghini et al, 2021) by removing Illumina adapters provided in the Nextera-PE.fa file. Initially, Trimmomatic (Bolger et al, 2014) looked for seed matches (16 bases) allowing a maximum of 2 mismatches. These seeds were extended and clipped if, in the case of paired end reads, a score of 30 was reached (approximately 50 bases). The reads were scanned with a 4-base wide sliding window, cutting when the average quality per base dropped below the trimming position with a Phred score <20 and discarding reads shorter than 50 nt. Human DNA was removed using Bowtie2 (Langmead and Salzberg,

2012) to map the reads against the reference genomes (*Homo sapiens* hg37 reference database). All metagenomes have been deposited in the European Nucleotide Archive at EMBL-European Bioinformatics Institute under accession number PRJEB67362.

Taxonomic and functional profiling. Metagenomic taxonomic profiles were obtained using MetaPhlAn 4 (Blanco-Míguez et al, 2023), a tool that maps shotgun reads to a database of unique clade-specific markers (mpa_vOct22_CHOCOPhlanSGB_202212) and is capable of producing species-level resolution and the relative abundances of each species per clade in a sample. We adjusted 1 parameter from the default parameter settings; the quantile value for the robust average (stat_q) was set to 0.1 to perform a more sensitive profiling. This parameter is used when MetaPhlAn calculates the robust average coverage of a species and defines the trimming of the marker distribution at both ends (Beghini et al, 2021). The profiling results are based on the fraction of reads mapping against the taxonomically unique species-specific MetaPhlAn 4 markers (± 5.1 M unique clade-specific marker genes). To functionally profile the metagenomes, we used HUMAnN, version 3.6 (using the database mpa_vJan21_CHOCOPhlanSGB_202103). Nucleotide subject coverage and translated subject coverage thresholds were set to 0 to turn off the coverage filtering and increase the number of reads that hit the pangenome.

Specialized gene family alignments were conducted using Diamond BLASTX (Buchfink et al, 2021) to annotate virulence factors (VFs) and antimicrobial resistance (AMR) elements. The BLASTx searches were run against the 2022 VF database (Liu et al, 2022) and the comprehensive antibiotic resistance database (Alcock et al, 2020). The E-value thresholds to call a hit were based on the median E-value of BLASTX searches of 10 samples whose reads were shuffled (to retain nucleotide proportions but randomize order) (Supplementary Figure S13). The lowest E-value per read was retained, and sequence variants within gene families were aggregated to result in VF and AMR element abundance tables. VFs were annotated on the basis of the empirical E-value threshold of 4.87×10^{-4} and had a mean (SD) coverage and percentage identity of 84.7 ± 16.1 and 52.9 ± 13.3 , respectively. Analogously, AMR genes were annotated on the basis of E-values below the empirical threshold of 4.32×10^{-4} with a mean (SD) coverage and percentage identity of 82.5 ± 16.0 and 50.5 ± 14.4 , respectively.

Statistical data analysis

Diversity analysis. The Wilcoxon signed rank test was used to assess differences in observed richness, Shannon diversity, Simpson evenness, and Gini index. For the calculation of the diversity metrics, the package microbiome (version 1.20.0) (Lahti and Shetty, 2012–2019) was used, and the false discovery rate-adjusted P-values were obtained using the p.adjust function. We performed multivariate ANOVA with the adonis2 function in the vegan R package (version 2.6-4) (Oksanen et al, 2024) to test for effect size and significance of predictor variables on Jaccard and Bray–Curtis dissimilarity matrices. To account for the potential interindividual effect, the model included study participant (subjectID) as a

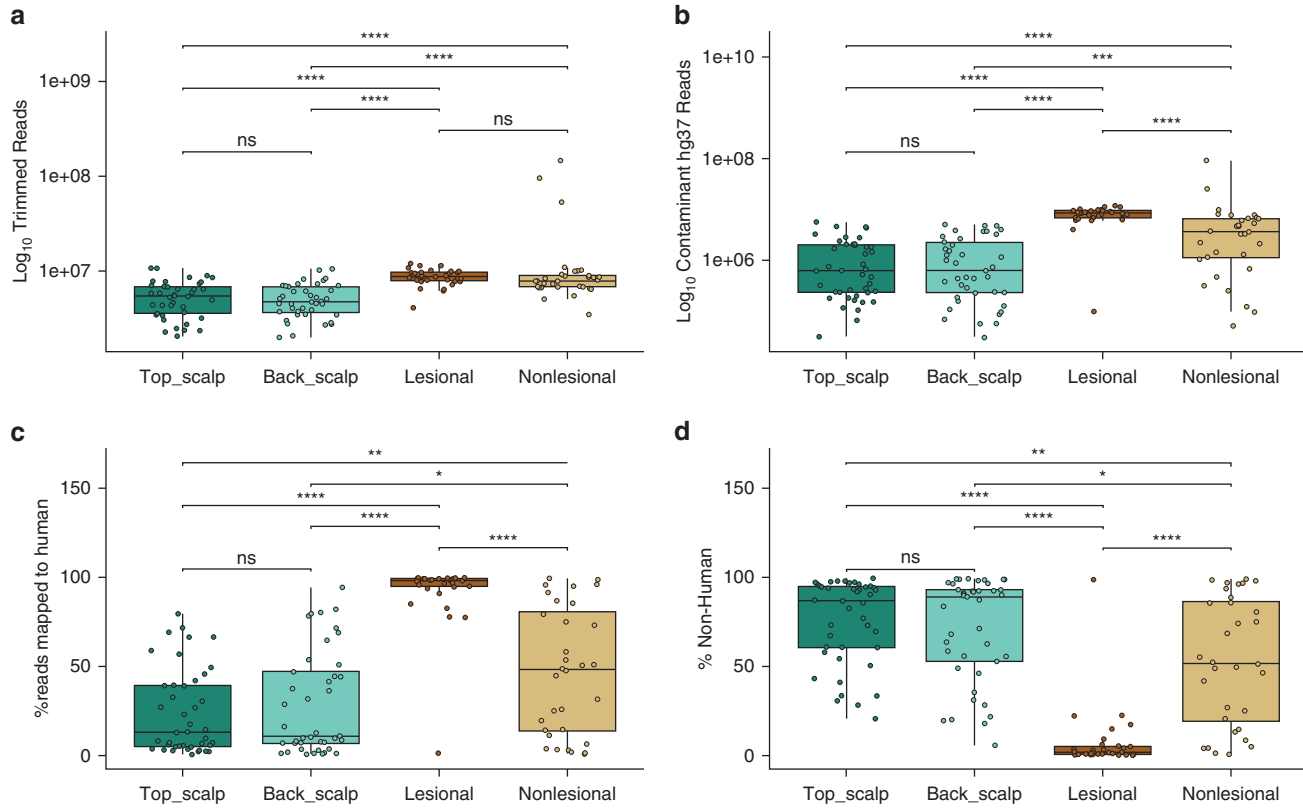
predictor variable, when necessary, followed by the Body_site variable ($\text{distance_matrix} \sim \text{subjectID} + \text{body_site}$). The tests were run for 999 default permutations, the false discovery rate-adjusted P -values were obtained using the `p.adjust` function, and adjusted R^2 was calculated using the `varpart` function (`vegan`). Jaccard and Bray–Curtis dissimilarity matrices were calculated with the `vegdist` function (`vegan`) on the relative abundance of metagenomic species. Dissimilarity matrices were subjected to classical multidimensional scaling (principal coordinate analysis) to obtain the principal coordinates and the variance explained by each coordinate. We assessed the multivariate homogeneity of group dispersions (variances) using the `betadisper` function (`vegan`) ([Supplementary Table S4](#)). In addition, we performed robust principal component analysis on the unrarefied read statistics (ie, the raw sequencing read counts without rarefaction) because there was no significant difference when performing robust principal component analysis on the rarefied read statistics ([Martino et al., 2022](#)). Permutational multivariate ANOVA calculation was performed using `scikit-bio` to determine statistical significance between all 4 groups.

Scalp microbiome biomarker analysis. We applied MaAsLin 2.0 ([Mallick et al., 2021](#)) method to identify microbial features, functional pathways, VF genes, and AMR genes that were associated with psoriasis (lesional or nonlesional) or healthy (top or back) scalp microbiomes. For that, we used a variety of data types, including metagenome-based taxonomic profiles, metagenome functional profiles, VF genes, and AMR gene element relative abundance tables. We applied default method implementation using a log-transformed linear model on total sum scaling—normalized quality-controlled data, accounting for interindividual variability by specifying between-participant random effects in the model when samples were obtained from the same participant. We only looked at those features (species,

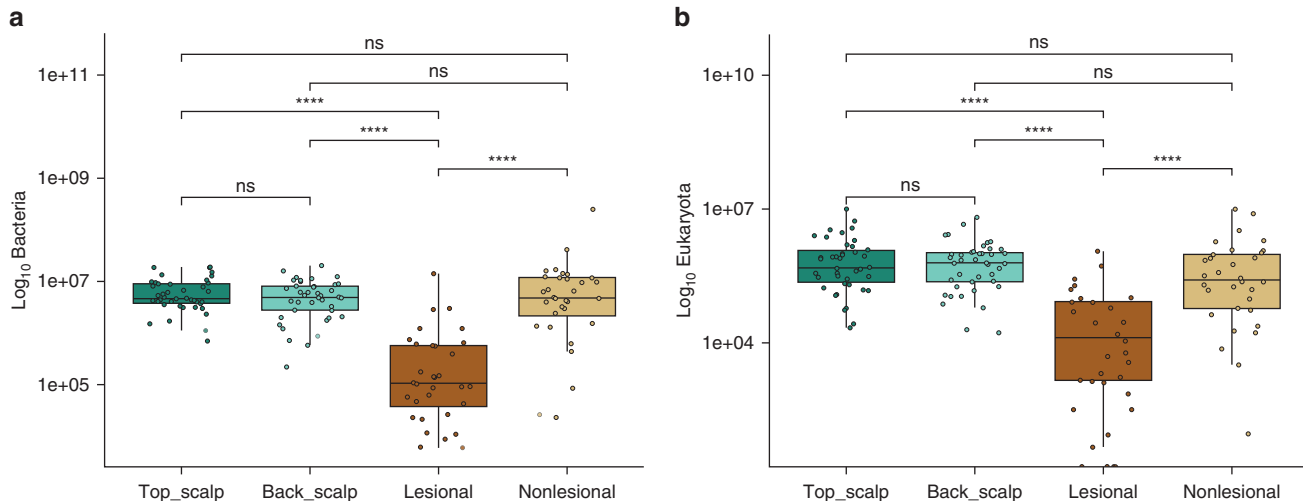
pathways, VF genes, AMR genes) that occurred in at least 10% of the samples and had a minimum abundance of 0.01%. All associations were corrected for multiple hypothesis testing using the Benjamini–Hochberg method, declaring significant associations at a target false discovery rate of 0.05.

SUPPLEMENTARY REFERENCES

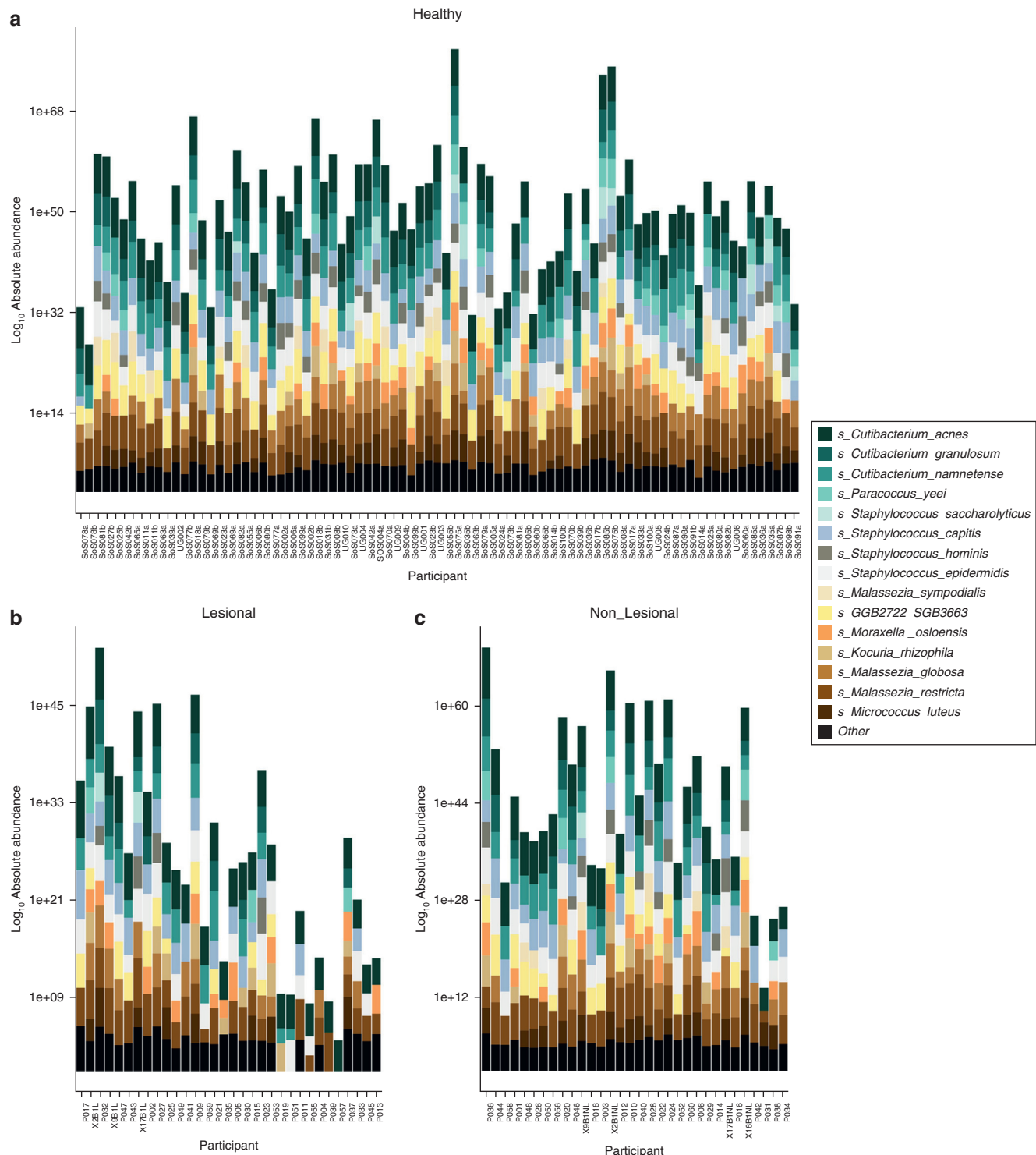
- Alcock BP, Raphena AR, Lau TTY, Tsang KK, Bouchard M, Edalatmand A, et al. CARD 2020: antibiotic resistance surveillance with the comprehensive antibiotic resistance database. *Nucleic Acids Res* 2020;48:D517–25.
- Beghini F, McIver LJ, Blanco-Míguez A, Dubois L, Asnicar F, Maharjan S, et al. Integrating taxonomic, functional, and strain-level profiling of diverse microbial communities with bioBakery 3. *eLife* 2021;10:e65088.
- Blanco-Míguez A, Beghini F, Cumbo F, McIver LJ, Thompson KN, Zolfo M, et al. Extending and improving metagenomic taxonomic profiling with uncharacterized species using MetaPhlAn 4. *Nat Biotechnol* 2023;41: 1633–44.
- Bolger AM, Lohse M, Usadel B. Trimmomatic: a flexible trimmer for Illumina sequence data. *Bioinformatics* 2014;30:2114–20.
- Buchfink B, Reuter K, Drost HG. Sensitive protein alignments at tree-of-life scale using DIAMOND. *Nat Methods* 2021;18:366–8.
- Lahti L, Shetty S. microbiome R package. <https://www.bioconductor.org/packages/release/bioc/html/microbiome.html>. (accessed September 10, 2024). 2012–2019.
- Langmead B, Salzberg SL. Fast gapped-read alignment with Bowtie 2. *Nat Methods* 2012;9:357–9.
- Liu B, Zheng D, Zhou S, Chen L, Yang J. VFDB 2022: a general classification scheme for bacterial virulence factors. *Nucleic Acids Res* 2022;50: D912–7.
- Mallick H, Rahnavard A, McIver LJ, Ma S, Zhang Y, Nguyen LH, et al. Multivariable association discovery in population-scale meta-omics studies. *PLoS Comput Biol* 2021;17:e1009442.
- Martino C, McDonald D, Cantrell K, Dilmore AH, Vázquez-Baeza Y, Shenhav L, et al. Compositionally aware phylogenetic beta-diversity measures better resolve microbiomes associated with phenotype. *mSystems* 2022;7:e0005022.
- Oksanen J, Simpson GL, Blanchet FG, Kindt R, Legendre P, Minchin PR, et al. Package ‘vegan’. <https://cran.r-project.org/web/packages/vegan/vegan.pdf>; 2024. (accessed September 10, 2024).



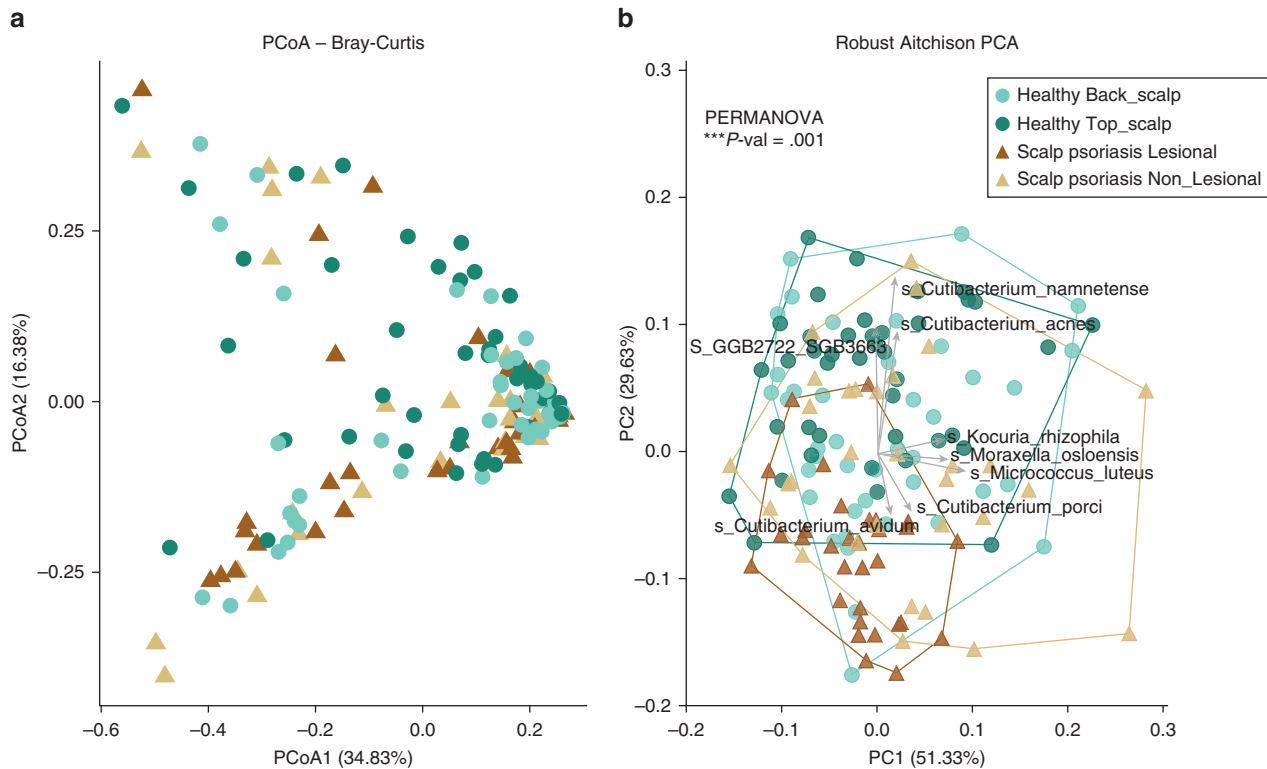
Supplementary Figure S1. Boxplots for each scalp skin site. Boxplots show the (a) the number of trimmed reads after running Trimmomatic on a log₁₀-transformed y-axis, (b) the number of human reads after mapping to the human reference genome database (hg37) on a log₁₀-transformed y-axis, (c) percentage of reads mapping to the human reference genome database (hg37), and (d) percentage of reads not mapping to the human reference genome database (hg37). Line in boxplots indicates median; boxes represent first and third quartiles. Sites are colored by site characteristic: top and back scalp areas from healthy participants and lesional and nonlesional scalp areas from participants with psoriasis capitis. A nonparametric Wilcoxon test was performed. Asterisks indicate the significance level of the FDR-adjusted *P*-values: *****P* < .0001, ****P* < .001, ***P* < .01, and **P* < .05. FDR, false discovery rate; ns, nonsignificant.



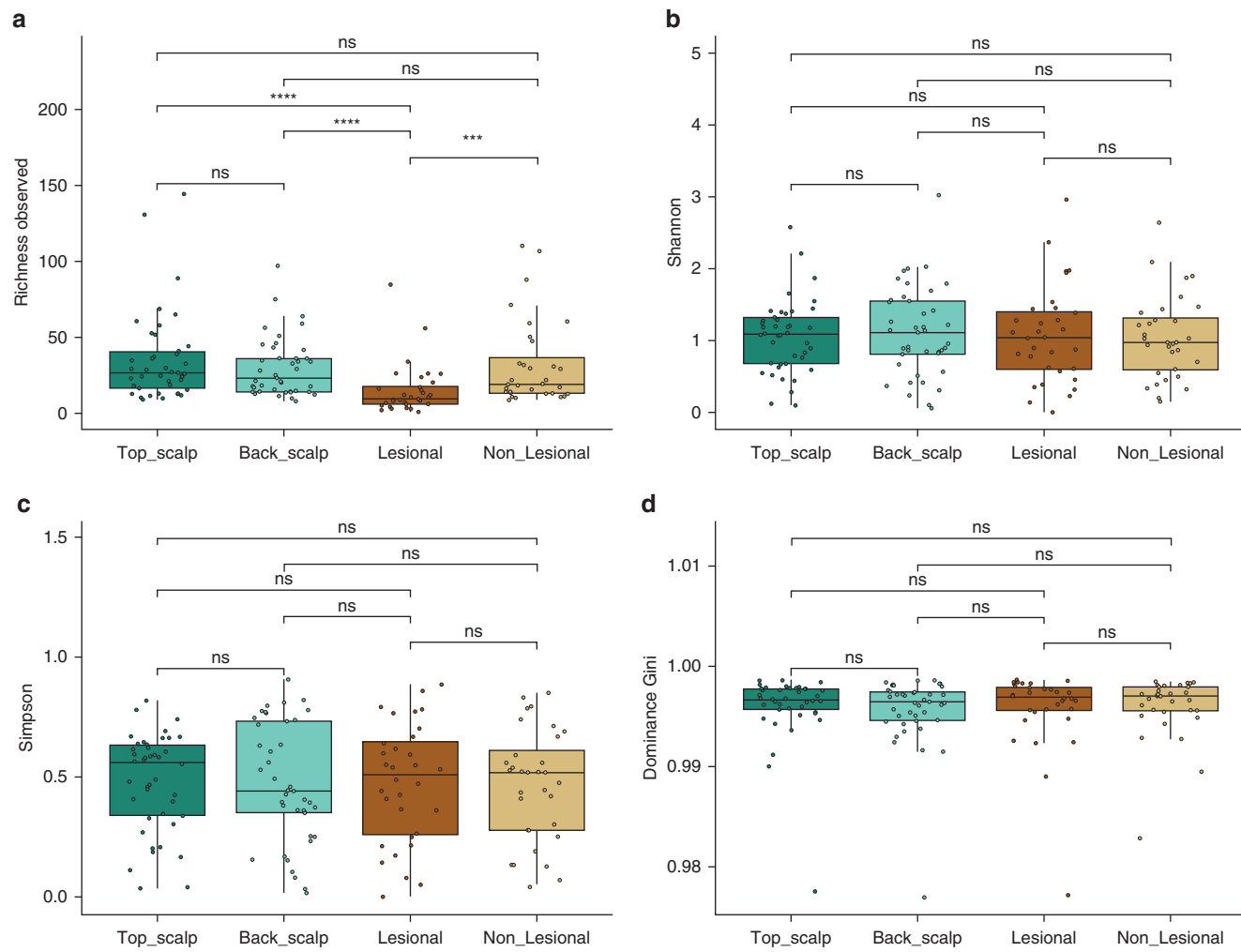
Supplementary Figure S2. Boxplots (line indicates median; boxes represent first and third quartiles) show, for each site, on a log₁₀-transformed y-axis, the estimated number of reads coming from bacteria and the estimated number of reads coming from eukaryota. (a) bacteria. (b) eukaryota. Sites are colored by site characteristic. A nonparametric Wilcoxon test was performed. Asterisks indicate the significance level of FDR-adjusted *P*-values: *****P* < .0001, ****P* < .001, ***P* < .01, and **P* < .05. FDR, false discovery rate; ns, nonsignificant.



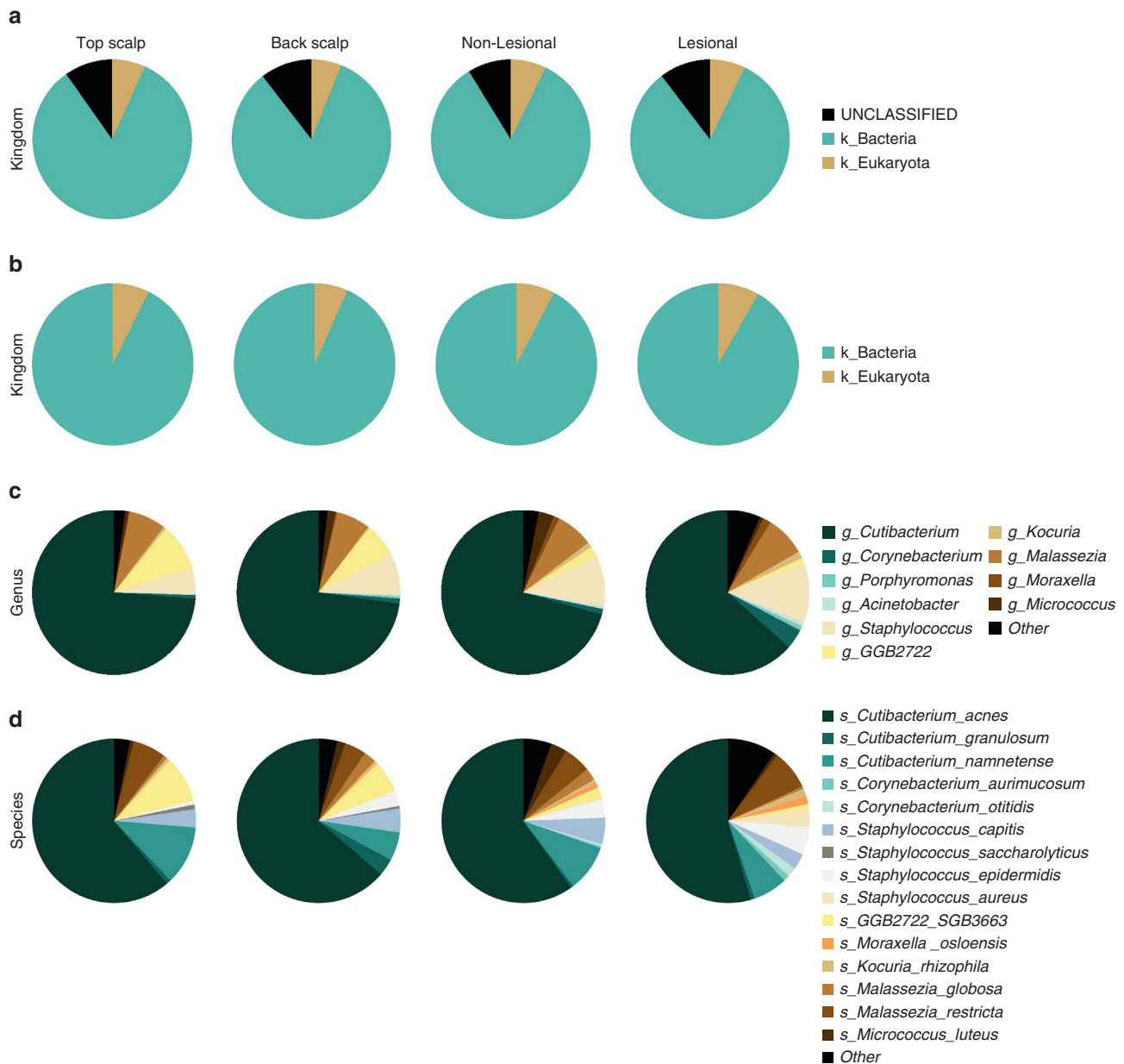
Supplementary Figure S3. Estimated number of reads coming from each clade of the 15 most commonly kSGBs and uSGBs ordered by *Cutibacterium acnes'* relative abundance. (a) Healthy individuals. (b) Lesional scalp areas. (c) Nonlesional scalp areas of individuals with psoriasis on a log₁₀-transformed y-axis. kSGB, known species-level genome bin; uSGB, unknown species-level genome bin.



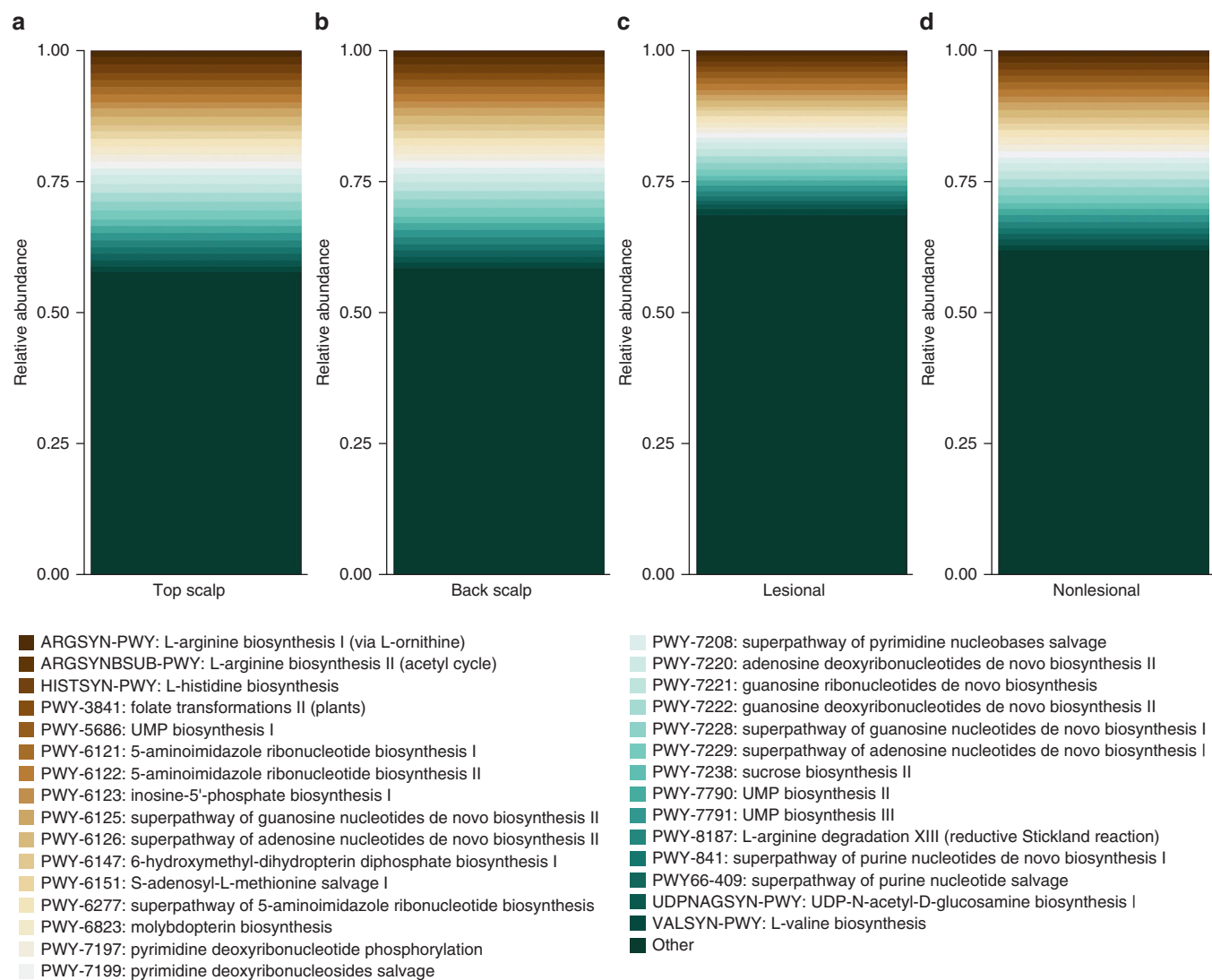
Supplementary Figure S4. Beta diversity analysis. (a) PCoA performed on the metagenomic species Bray–Curtis matrix calculated on the relative abundance of features. (b) Robust Aitchison PCA performed on the species feature table derived from unrefined read statistics (ie, the raw sequencing read counts without rarefaction). Significance testing between groups was conducted using PERMANOVA. Top features are shown on the biplot. The percentage explained by principal coordinates 1 and 2 is included in the axis labels. PC1, principal component 1; PC2, principal component 2; PCA, principal component analysis; PCoA, principal coordinates analysis; PERMANOVA, permutational multivariate ANOVA.



Supplementary Figure S5. Alpha diversity boxplots (line indicates median; boxes represent first and third quartiles). (a) The total number of species (richness observed), (b) the number of species and species evenness (Shannon), (c) species evenness (Simpson), and (d) dominance or inequality (dominance Gini). A nonparametric Wilcoxon test was performed. Asterisks indicate the significance level of the FDR-adjusted P -values: **** $P < .0001$, *** $P < .001$, ** $P < .01$, and * $P < .05$. FDR, false discovery rate; ns, nonsignificant.

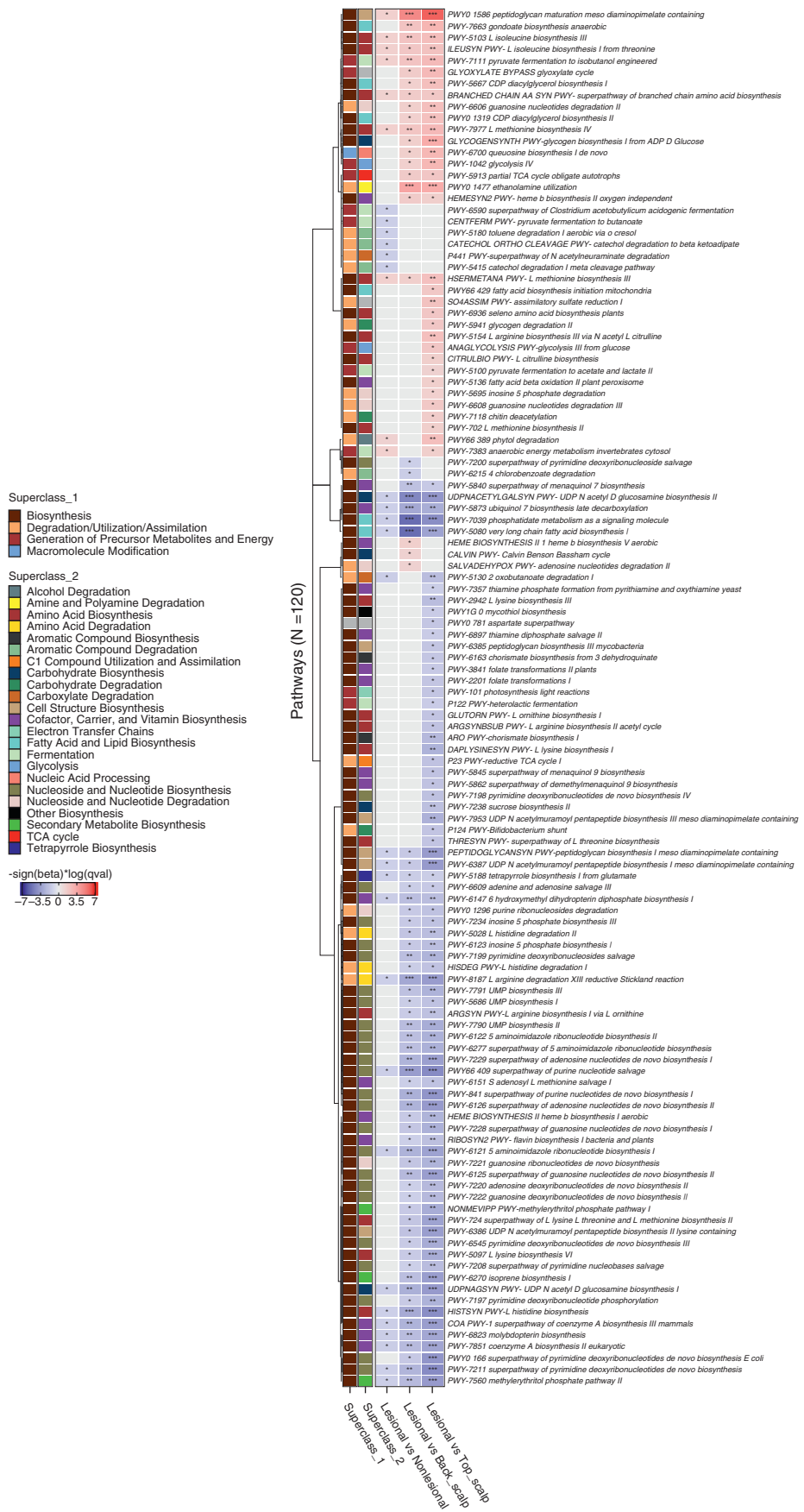


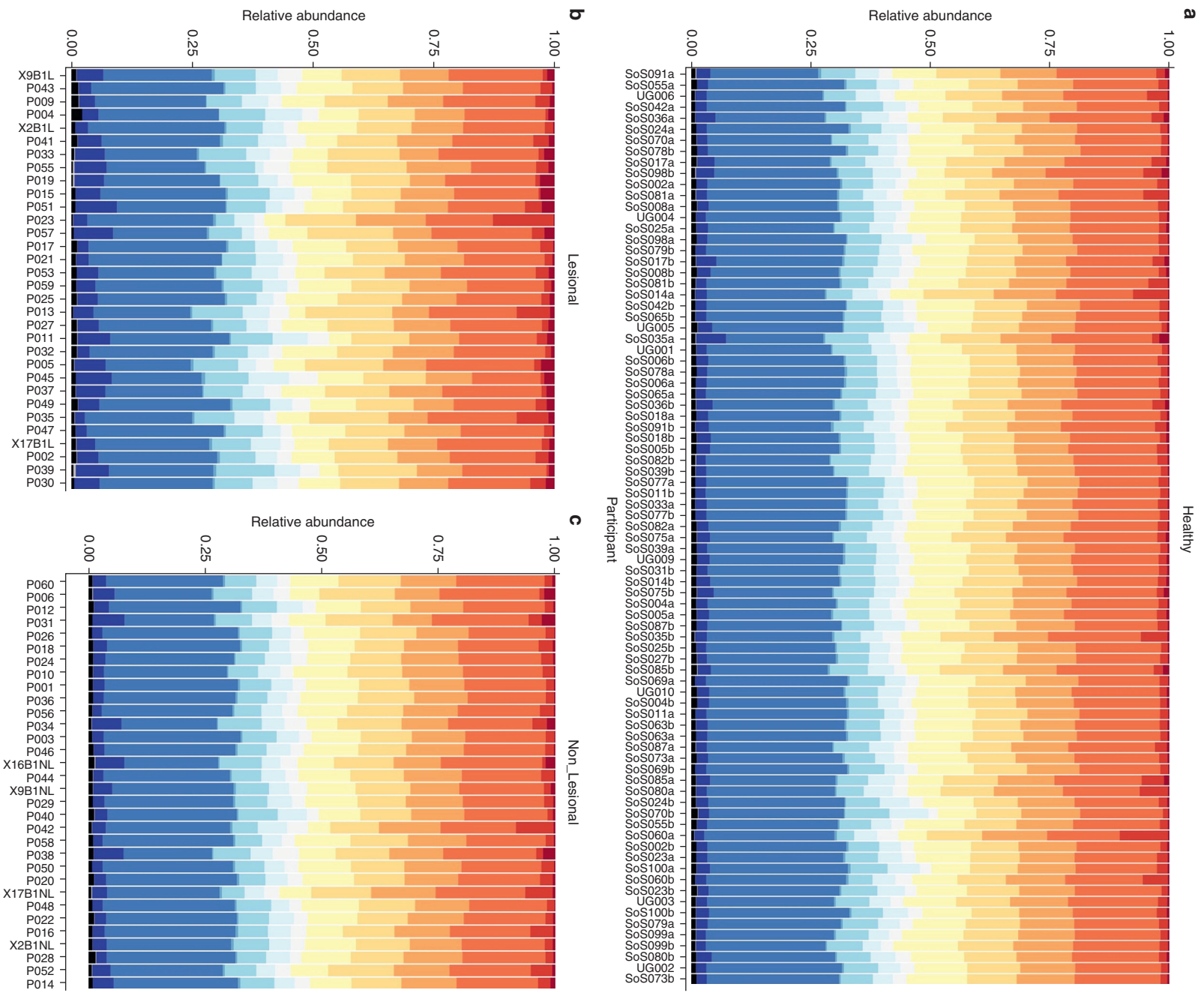
Supplementary Figure S6. Average relative abundance. (a) Kingdom (with unclassified fraction). (b) Kingdom (excluding unclassified fraction). (c) Top 10 genera. (d) Top 15 species stratified by sample group. The top and back scalp areas are from healthy participants ($n = 43$), and the nonlesional and lesional scalp areas are from participants with psoriasis capitis ($n = 33$).



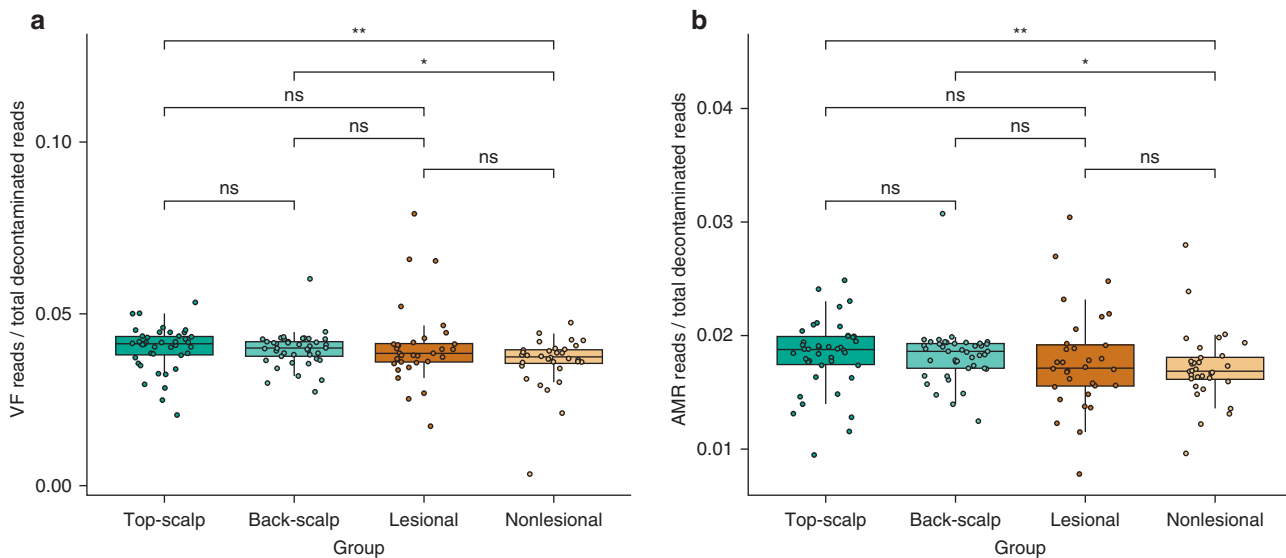
Supplementary Figure S7. Average relative abundance of the 30 most common functional pathways stratified by sample group. (a) Top and (b) back scalp areas from healthy participants ($n = 43$) and (c) lesional and (d) nonlesional scalp areas from participants with psoriasis capitis ($n = 33$).

Supplementary Figure S8. Functional pathways (N = 120) associated with lesional scalp areas compared with those associated with nonlesional scalp areas, the back of the scalp, and the top of the scalp. Representative significant pathway associations (FDR < 0.05) detected by MaAsLin 2.0's default linear mixed effects model are shown. All detected associations were adjusted for body site as a fixed effect and adjusted for subjectID when samples were obtained from the same participant. Values are log-transformed relative abundances. Complete linkage clustering of Pearson correlation coefficients was used to hierarchically cluster the features. Asterisks indicate the significance level of FDR-adjusted *P*-values: ****P* < .001, ***P* < .01, and **P* < .05. FDR, false discovery rate.

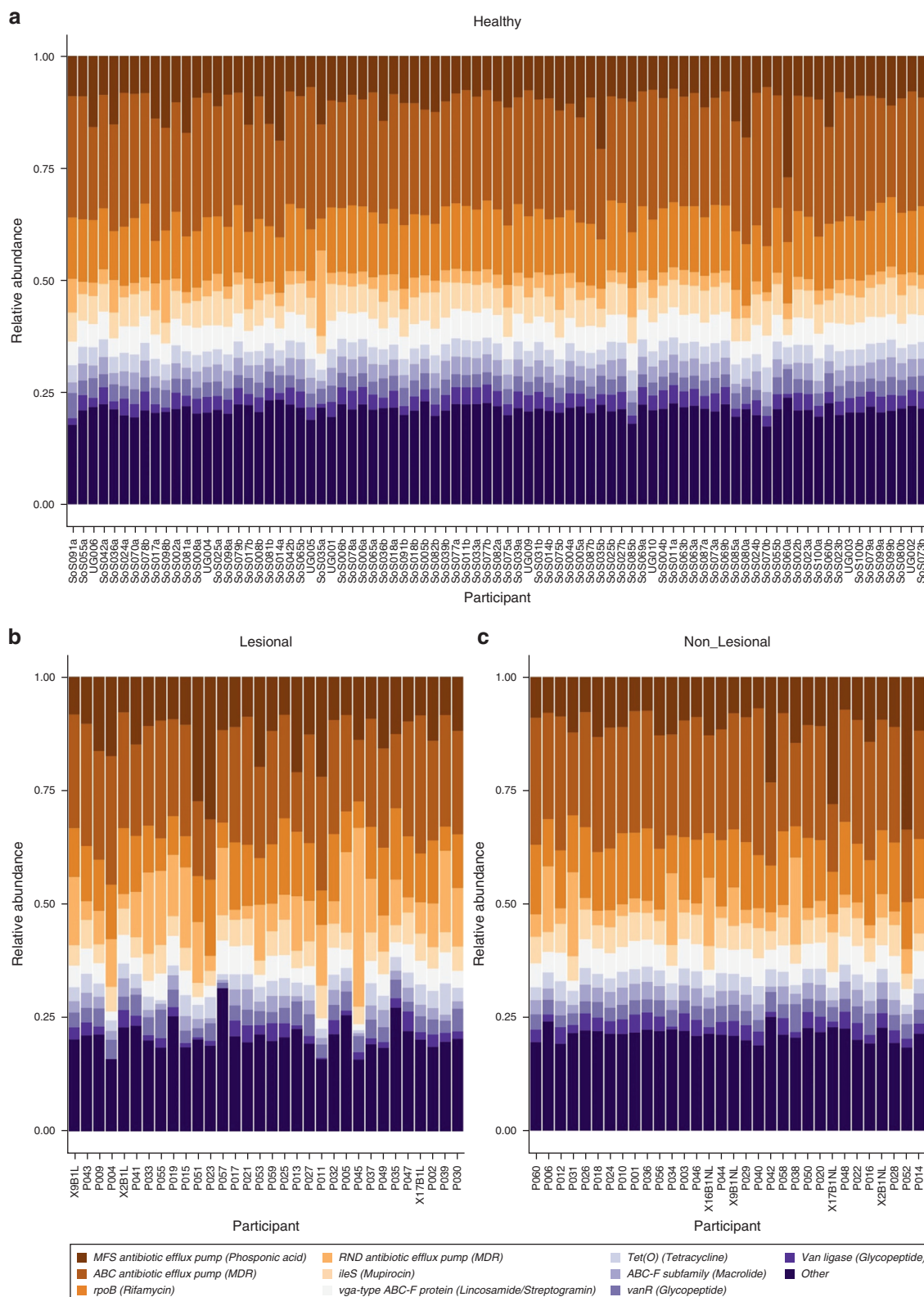




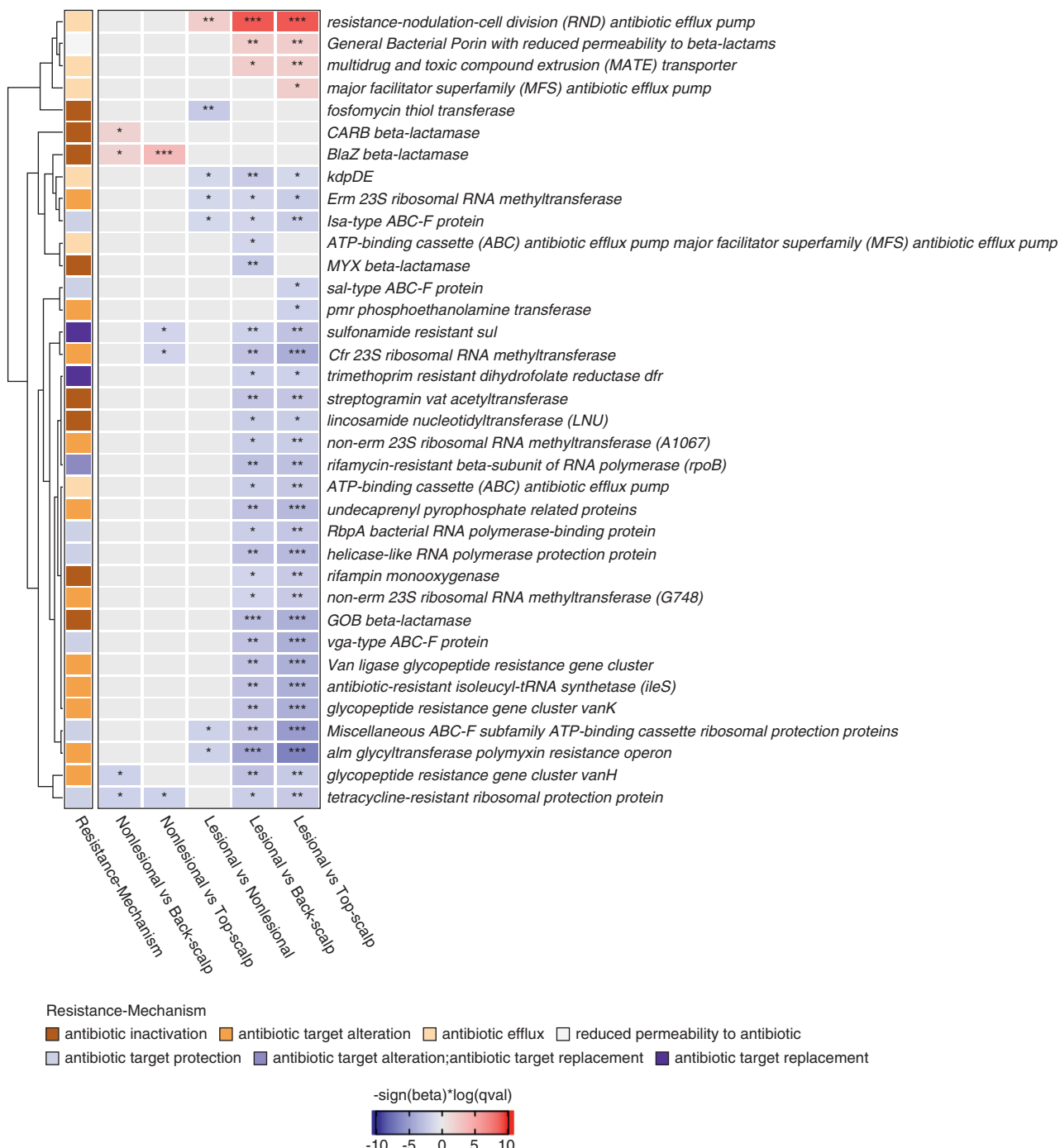
Supplementary Figure S9. Relative VF abundance per VF class stratified by sample group. (a) Healthy; (b) Lesional; (c) Nonlesional. VF, virulence factor.



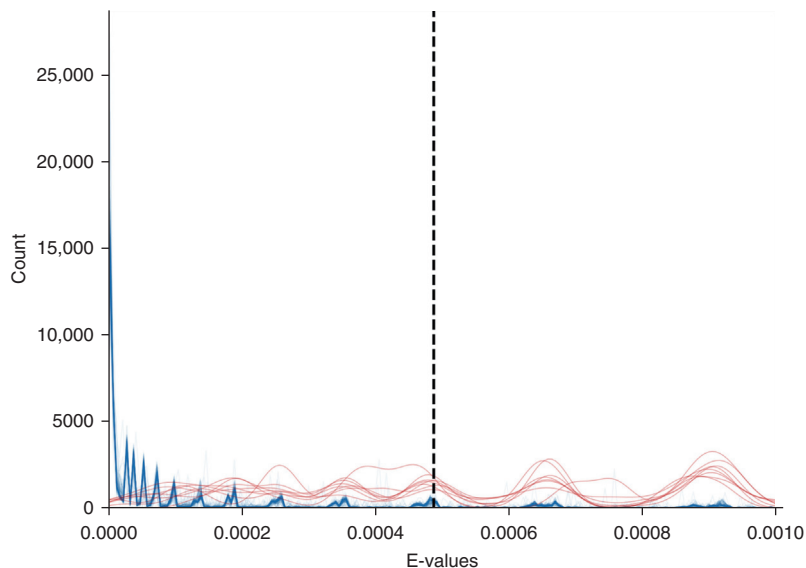
Supplementary Figure S10. Boxplots (line indicates median; boxes represent first and third quartiles) show, for each site, the number of VF reads divided by the total number of decontaminated reads per sample and the number of AMR gene reads divided by the total number of decontaminated reads per sample. (a) VF reads divided by the total number of decontaminated reads per sample. (b) AMR gene reads divided by the total number of decontaminated reads per sample. Sites are colored by site characteristic. A nonparametric Wilcoxon test was performed. Asterisks indicate the significance level of the FDR-adjusted P -values: *** $P < .001$, ** $P < .01$, and * $P < .05$. AMR, antimicrobial resistance; FDR, false discovery rate; ns, nonsignificant; VF, virulence factor.



Supplementary Figure S11. Relative abundance of the 10 most common AMR genes, stratified by sample group. (a) Healthy. (b) Lesional. (c) Nonlesional. AMR gene abbreviations include MFS for major facilitator superfamily, ABC for adenosine triphosphate-binding cassette, MDR for multidrug resistance, rpoB for rifamycin-resistant beta-subunit of RNA polymerase, RND for resistance nodulation division, ileS for antibiotic-resistant isoleucyl-tRNA synthetase, Tet(O) for tetracycline-resistant ribosomal protection protein, vanR for glycopeptide resistance gene cluster, and Van Ligase for glycopeptide resistance gene cluster. AMR, antimicrobial resistance.



Supplementary Figure S12. Representative significant AMR gene associations (FDR < 0.05) detected by MaAsLin 2.0's default linear mixed effects model (n = 36) and their resistance mechanism. All detected associations were adjusted for body site as a fixed effect and adjusted for subjectID when samples were obtained from the same participant. Values are log-transformed relative abundances. Complete linkage clustering of Pearson correlation coefficients was used to hierarchically cluster the features. Asterisks indicate the significance level of FDR-adjusted P-values: ***P < .001, **P < .01, *P < .05. AMR, antimicrobial resistance; FDR, false discovery rate.

a

Supplementary Figure S13.
Determination of the E-value thresholds based on the median E-value of BLASTX searches of 10 samples whose reads were shuffled (to retain nucleotide proportions but randomize order). (a) VF genes and (b) AMR genes. The lowest E-value per read was retained, and sequence variants within gene families were aggregated to result in VF and AMR element abundance tables. AMR, antimicrobial resistance; VF, virulence factor.

b